6. Snow cover and Snowfall

6.1 Estimating snow water equivalent in alpine snowpacks: Methods, strategies, and sources of variability

G. Filippa[1], U. Morra di Cella[1], E. Cremonese[1], P. Pogliotti[1], F. Diotri[1], M. Isabellon[1]

[1]*ARPA Valle d'Aosta, Aosta, Italy*

6.1.1 Background

The accurate estimation of snow water equivalent (SWE) for alpine regions is a crucial information for a number of applications, like e.g. hydro-power production, water resources management, or artificial snow production (Clarvis et al., 2013). While automatic snow depth (HS) sensors are widespread and deployed in mountain ranges worldwide, this is not the case yet for SWE sensors (Smith et al., 2017). Indeed, frequent and well distributed manual measurements of bulk snow density (RHO), used to convert HS in SWE, are still needed. For this purpose, observers are trained and observation networks are deployed in the Alps to provide weekly or sometimes daily, measurements of SWE. These measurements are challenging due to the harsh environmental conditions, rugged terrain, remoteness of the sampling locations and observer's security (e.g., risk of avalanches). It is therefore desirable to optimize the measurement strategy by reducing the sampling effort in order to achieve a given target of accuracy (Lopèz-Moreno et al., 2011; Molotch et al., 2005).

In the Italian Alps, three methods are used to measure SWE: *1)* the AINEVA protocol (Mod. 3-4), based on the recognition of discrete strata in the snowpack, the measure of RHO for each stratum and the profile-average weighted mean. This method was developed for the accurate description of the snowpack, including grain size, metamorphism and snow stability assessment for avalanche bulletins; *2)* the simple method (SIMPLE), where RHO is measured at fixed depths in the snowpack and averaged. This method was specifically designed for SWE measurements and does not require expertise in snow profile description, such as grain recognition; *3)* the CORE method consists of sampling a vertical snow core of known volume, returning a profile-integrated SWE measurement. This fast and easy-to-use method was specifically developed by hydropower production companies and deployed since the early 40s.

Year	***N***	***Sampling strategy***	***Objectives***	***Location***
March 5th, 2015	186	On a 1000 m^2 plot three 15 m-long-transects were defined and sampled with two different methods (AINEVA and SIMPLE).	i) quantify observer and inter-observer error under rather homogeneous snow conditions ii) estimate variability b/w methods under rather homogeneous snow conditions	Pila, Aosta Valley, Italy, 2250 m ASL
March 3rd, 2016	184 48	On a 500 m^2 plot 4 cubes of 5 m-side were sampled on each side with two different methods (AINEVA/SIMPLE and CORE)	i) quantify observer and inter-observer error under homogeneous snow conditions ii) estimate variability b/w method s under homogeneous snow conditions	Santa Caterina Valfurva, Lombardia, Italy, 2750 m ASL

		On 8 sampling points along a spatially heterogeneous slope with two different methods	iii) optimize the sampling strategy	
March 19th, 2018	93	On a 58 km^2 basin SWE was determined at different elevations, slopes and facing.	i) evaluate the relationship between SWE and dem-derived variables ii) optimize the sampling strategy	Bardonecchia, Piemonte, Italy, elevation range 1300-2800 m ASL

Table 1. *Summary of the three SWE campaigns described in this study. N is the number of observations.*

By means of 3 field campaigns involving a large number of observers conducted in 2015, 2016 and 2018 (Table 1), we aimed to:

i) evaluate the inter-comparability between the above described three different methods (campaigns 2015 and 2016);

ii) quantify the measurement error associated with the observer (campaigns 2015 and 2016);

iii) describe the spatial variability of SWE at different scales (2015, 2016, 2018);

iv) estimate the appropriate number of measurements required to achieve a given target of accuracy in SWE measurements (2016, 2018).

6.1.2 Results

Each campaign was designed and tuned based on the outcome of the previous experience; therefore, in the following paragraph we will illustrate the results of each campaign.

2015

SWE was measured along three 15m-transects in a homogeneous snowfield of about 1000 m^2 (186 points sampled). Measurements were conducted by 17 couples of observers. In each couple, one operator consistently made the measurements, while the other assisted the first. The same observer took two measurements per transect close to each other, and the resulting variability was used as an estimate of the operator error. The variability between the 17 couples of observers was used as an estimate of the inter-operator error. The variability between the three transects was used as an estimate of the spatial variability.

An average of 280 mm, 98 cm, and 300 kg m^{-3} for SWE, HS and RHO, respectively, was measured.

We calculated that the same observer taking two SWE measurements on a snowpack under similar conditions and using the same methods makes an average measurement error of 2.5% (around 7 mm SWE). The inter-observer variability is quantified at 10% (28 mm SWE) and the spatial variability between the three transects was around 6% (17 mm). The variability between the two methods (AINEVA and SIMPLE) was low, at 3.8% (11 mm). A t-test indicates that the two methods lead to the same estimated SWE.

The inter-observer variability, the highest found in this campaign, highlights the need for further inter-comparisons aiming at the homogenization of sampling techniques. It has however to be noted that we assumed each transect as homogeneous and therefore attributed the within-transect variability to measurement errors of the observers only, but it was likely that the 15-m transects could have an intrinsic spatial variability that was not accounted for in our experimental design. This problem was addressed explicitly in the 2016 campaign.

2016

SWE was measured on the sides of four cubes of 5-m side in a homogeneous snowfield of about 1000 m^2 (184 points sampled). We chose this sampling design in order to minimize the distance between different observations and therefore avoid unaccounted spatial variability within each single cube. Measurements were performed with the snow profile methods (either AINEVA and SIMPLE, found to be identical in 2015 campaign), and with the snow core method (CORE, cfr. Background). We measured global averages of 390 mm, 135 cm, and 290 kg m^{-3} for SWE, HS and RHO, respectively.
We calculated that the same observer taking SWE measurements on a homogeneous snowpack makes an average error of 3% (around 11 mm SWE), in line with the results of the 2015 campaign. The inter-observer variability was 10% (39 mm SWE). The spatial variability of the four cubes was 7.4% (29 mm). The variability between the two methods (AINEVA/SIMPLE and CORE) was 6.6% (26 mm SWE).
A t-test demonstrated that both methods lead to a correct estimate of the ground truth, defined as the global average of all measurements.
In order to translate the experiment into operational protocols, we tested how much we can reduce the sampling effort without losing statistical power in properly determining the ground truth. We used a re-sampling technique, by randomly removing some observations and run the statistical tests on data subsets. Results are then expressed in probabilistic form (Figure 1). The graph shows the probability (%, x-axis) to obtain an SWE estimate equal to the ground truth (the global average of all measurements) as a function of sample size (y-axis). Different colors represent the two methods. Three samples are sufficient with both AINEVA/SIMPLE and CORE methods to correctly estimate the ground truth at a 95% confidence (a typical statistical threshold). In other words, in face of a homogeneous snow field, the average of 3 samples would give us a 95% probability of retrieving the true SWE of that area.

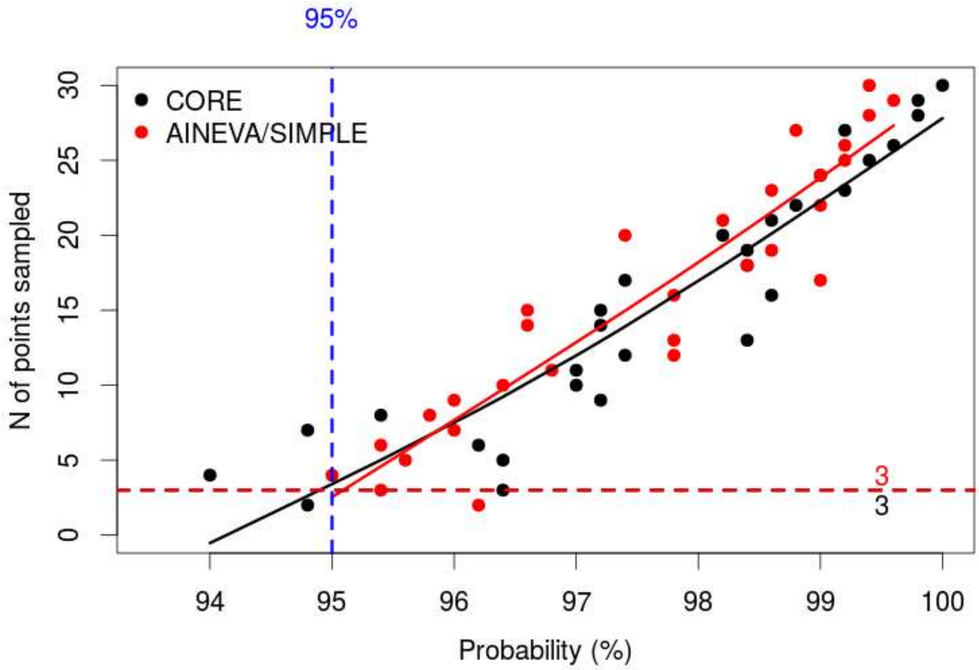

Figure 1. *Results of the re-sampling experiment. Variation of the probability to obtain a correct estimate of the SWE as a function of number of points sampled.*

In addition to the work conducted on the homogeneous snowfield, SWE was also measured across a slope in 8 sampling points with several repetitions, resulting in 48 measurements. SWE, in this small slope, ranged between 170 and 350 mm. Mean spatial variability here was much higher (34%, 80 mm SWE), whereas the variability due to the two methods was similar to the one observed in homogeneous conditions (24 mm, 10%). The same re-sampling approach, illustrated above, was used to calculate the minimum number of samples required to adequately estimate SWE in this slope. Results indicate that 6 or more samples are required to match the ground truth.

	HS [cm]	RHO [kg m-3]	SWE [mm]
Min	28	214	98
Median	168	339	550
Max	500	470	1984

Table 2. *Summary statistics of the measurements (n =93).*

2018

SWE was measured in a medium-scale basin (58 km^2). The 93 sampling points were chosen to cover 36 topographic units defined by combining classes of elevation, slope and aspect. In addition to SWE measurement, for each point, the observers classified the site according to snow erosion susceptibility as “erosion”, “accumulation” or “neutral”. Summary statistics of the measurements are reported in Table 2.

The first aim of this campaign was to determine the importance of topographic factors in the distribution of SWE. Results from a random forest analysis revealed that HS and SWE distribution were best explained by elevation (a positive relationship explaining 30% of the variation), followed by erosion, explaining an additional 20%. Snow bulk density (RHO) variability was best explained by potential radiation (that integrates slope and aspect) with higher values at higher incoming solar radiation. The performance of random forest models in the prediction of SWE and HS was much higher than for RHO (cross-validation R^2 equal to 0.40, 0.50, and 0.15 for SWE, HS and RHO, respectively). Further analyses demonstrated that, while below 2000 m elevation is the most important predictor of SWE distribution, at higher elevation snow erosion becomes the main determinant of SWE variability, because this is the altitudinal belt where erosion actually acts in modifying snow patterns.

The second aim of this campaign was to determine which sample size is needed to achieve a defined level of accuracy in SWE estimation for the whole area. Indeed, we progressively reduced the number of sampled points and computed the additional uncertainty related to the sample removal. We recall that SWE is the product of two distinct measurements: HS, which is simple and fast to be measured, and RHO, which is the labor-intense and time-consuming part of the measurement. The analysis was therefore run by reducing HS measurements and RHO measurements separately. Results are shown in Figure 2. Proceeding from right to left on the x-axis, sample number is reduced and uncertainty increases. The increase is more pronounced for HS than for RHO, because the variability range of HS is typically higher than for RHO, and HS is the major determinant of SWE variation. We can estimate that, for a target of error in SWE at 20% (which corresponds to 100 mm SWE), we need to design a sampling campaign with at least 70 HS measurements and 23 RHO measurements. If our uncertainty target was 10%, the number of samples required would clearly increase (Figure 2), but given that the inter-operator error under homogeneous conditions already totals 10% (2015 and 2016 campaign results) the target of 20% seems a more realistic objective in heterogeneous field conditions.

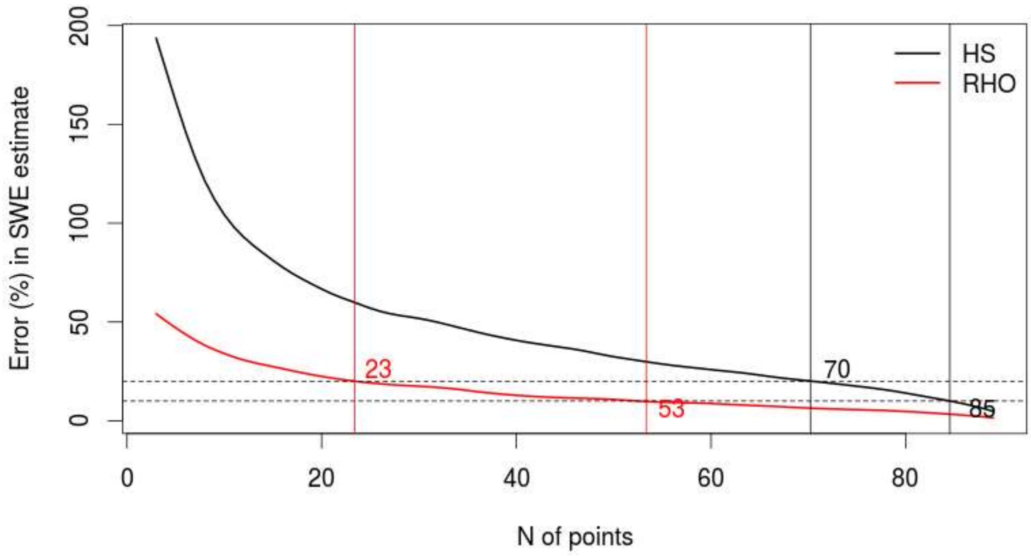

Figure 2. *Error in SWE estimate as a function of sample size for HS (black line) and RHO (red line). Annotations indicate the number of samples required for a given target of uncertainty (10 and 20%, indicated by the dashed horizontal lines).*

6.1.3 Summary

Three massive field campaigns, with different sampling designs and under different snow conditions, lead us to shed some light on sources of variability of SWE:

i) Operator error is a small and negligible fraction of the variability.

ii) Inter-operator error is an important fraction of variability, estimated at 10% of the mean SWE. This value can be viewed as the smallest discernible difference between different SWE estimates.

iii) We compared three different measurement methods (AINEVA, SIMPLE and CORE) and concluded that they provide similar SWE estimates.

iv) In a homogeneous snowfield, 3 sampling points are sufficient to properly quantify SWE. In a rather heterogeneous slope, the required points become 6.

v) At a medium-basin scale (58 km^2), we estimated that 70 HS samples and 23 RHO samples are needed to keep the uncertainty of mean basin SWE, around 20%. Indeed, we would roughly need a sampling density of 1 HS measurement per km^2 and 1 RHO measurement per 2 km^2, provided they give comprehensive coverage of the topographic characteristics of the basin. This last estimate must however be generalized with great caution, being the outcome of a single campaign and in one specific basin.

6.2 Snow cover and snowfall from satellite passive microwave sensors

V. Levizzani[1], S. Laviola[1]

[1]*CNR-ISAC, National Research Council, Institute of of Atmospheric Sciences and Climate, Bologna, Italy*

Measuring solid precipitation is crucial for several reasons including weather monitoring and forecasting, hydrology of high-latitude basins, but especially for closing the terrestrial water budget. Snowfall is hard to measure through ground-based gauges due to difficulty in discriminating between falling and resuspended snow, snow accumulation, icing of the sensors and error definition problems (e.g., Levizzani et al., 2011).

Snowfall observations from satellite have suffered of all the problems affecting rainfall estimates, but additional problems are related to:

- the distinction of ice hydrometeors from water drops making use also of the high frequency channels above 100 GHz;
- the complexity of the radiative properties of snowflakes and ice crystals;
- the poorly known cloud vertical structure and ice water content;
- the incomplete understanding of snow microphysics in mixed-phase clouds.

With the advent of high-frequency PMW radiometers such as the Advanced Microwave Sounding Unit-B (AMSU-B), snowfall has started to be detectable, although limitations persist since the ice content of a cloud is not known a priori. Physical models were developed to discriminate snowfall over land (e.g., Skofronick-Jackson et al., 2004). A most important problem to be solved is the detection of the snowfall signature over snow-covered ground. The advent of the GPM has recently shown that the combination of low (10-19 GHz) and high frequency (89-166 GHz) spectral bands of the GMI provides the maximum amount of information for snowfall detection (Ebtehaj and Kummerow, 2017). Operational algorithms have started to become available such as the one of NOAA (Meng et al., 2017), which has four components: cloud properties retrieval, computation of ice particle terminal velocity, ice water content adjustment, and the determination of snowfall rate. The algorithm is based on a 1D-Var approach and has been validated against radar and other ground-based observations. Several studies are being conducted using such radars and the GMI to quantify the detection skills of the instruments. You et al., (2017) have shown that scattering signatures are essential for snowfall detection. A statistical approach was adopted by Liu and Seo (2013), to correct precipitation retrievals where concentrations of high water vapour above the precipitation layer negated the scattering signatures in certain snowfall events. Inter-comparison exercises are being held to determine the potential of snowfall detection by the various algorithms (e.g., Laviola et al., 2015).

However, it is only with the combined availability of observations from the CPR on CloudSat and the GPM DPR that the research in this field has received a substantial boost. Skofronick-Jackson et al., (2013) determined the thresholds of detection for various active and passive sensor channel configurations and falling snow events over land surfaces and lakes, through model simulations of the minimum amount of snow using non-spherical snowflake shapes. Studies conducted on the snowfall detection capabilities of the DPR and more will become available soon (e.g., Casella et al., 2017; Panegrossi et al., 2017). The availability of CloudSat's CPR allowed to Liu, (2008) to conceive a derivation of snow-cloud characteristics in two steps: *1)* a snow-rain threshold based on multiyear land station and shipboard present weather reports, and *b)* a second part based on backscatter computations of non-spherical ice particles and in situ measured particle size distributions. The author found that the characteristics of the vertical distribution of snowfall rate are quite similar for over-ocean and over-land snow clouds, except that over-land snow clouds seem to be somewhat shallower than those over ocean. CloudSat has contributed to a global census of such shallow cumuliform snow clouds (Kulie et al., 2016; Kulie and Milani, 2018).

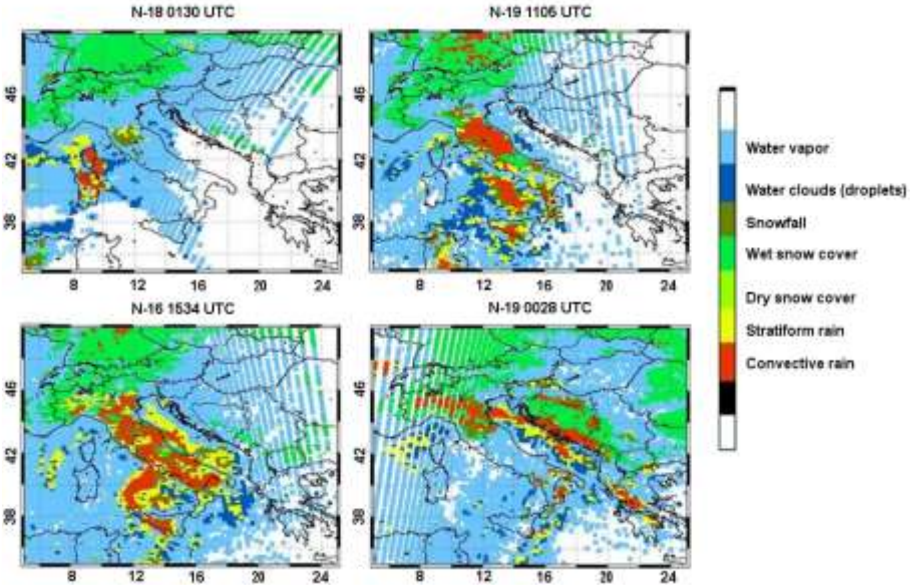

Figure 3. *Typical scene classification from the 183-WSL algorithm.*

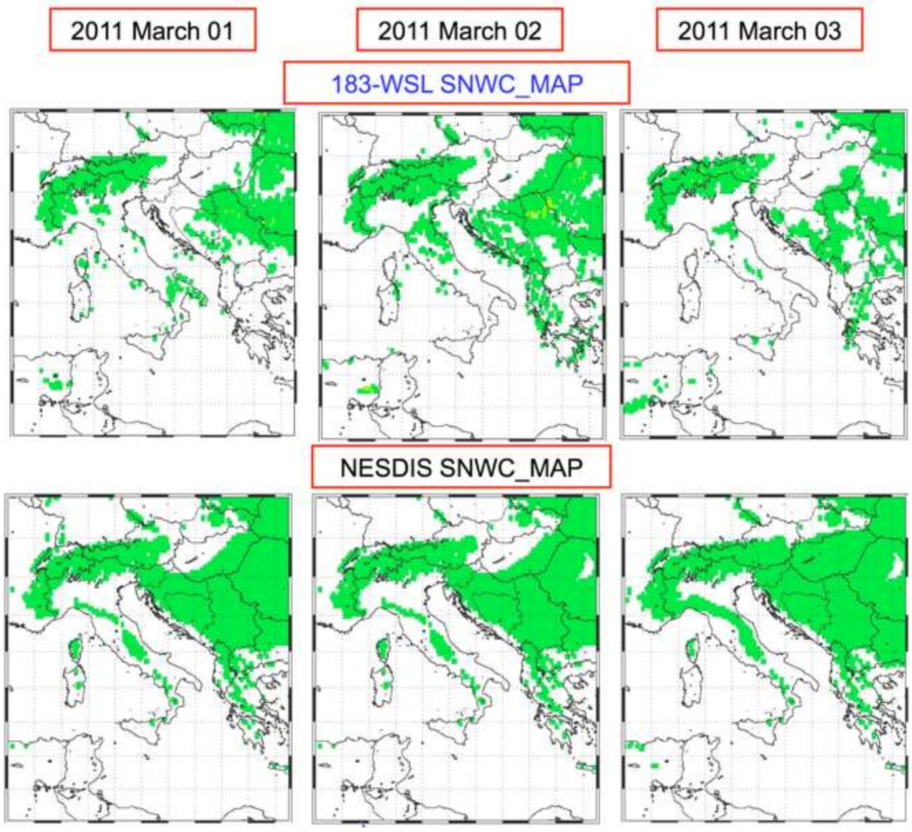

Figure 4. *Snow cover map from the 183-WSL algorithm (top plates) compared with the NOAA-NESDIS snow cover map (lower panels). Apparent underestimation is due to the fact that 183-WSL map is satellite-only while the NOAA product includes direct observations at the ground.*

During the project NextSnow, the precipitation retrieval algorithm Water vapour Strong Lines at 183 GHz (183-WSL) by Laviola and Levizzani, (2011) was modified and, a snowfall and snow cover detection module added and verified using independent data from the US and Europe. An example of cloud and snow detection is shown in Figure 3.
The algorithm is based on the sensitivity to snow- or ice-covered terrain of the window channels at 90 and 150 GHz combined with the scattering signal at 190 GHz. This snow module has shown clear skills in detecting snowfall over barren soil while in case of snow covered soil the separation of the scattering contribution of hydrometeors from that of ground snow still represents a problem. However, the variation of surface emissivity with water content and with snow physical state has allowed to characterize snow covered soils as a function of their humidity: fresh snow (or wet snow at high humidity content) and dry snow (typically stratified and compact with the uppermost layer completely glaciated). An example of retrieval of the snow cover in Figure 4.

6.3 Comparison of different snow models in an alpine test-site

S. Terzago[1], P. Pogliotti[2], E. Cremonese[2], U. Morra di Cella[2], S. Gabellani[3], G. Piazzi[3], D. Dolia[3], C. Cassardo[4], V. Andreoli[4], J. von Hardenberg[1], E. Palazzi[1], A. Provenzale[5]

[1]*CNR-ISAC, National Research Council of Italy, Institute of Atmospheric Sciences and Climate, Torino, Italy*
[2]*ARPA-Valle d'Aosta, Aosta, Italy*
[3]*CIMA Research Foundation, International Centre on Environmental Monitoring, Savona, Italy*
[4]*University of Torino, Department of Physics, Torino, Italy*
[5]*CNR-IGG, National Research Council of Italy, Institute of Geosciences and Earth Resources, Pisa, Italy*

Snow cover in high-altitude environments plays a key-role in terms of modification of the energy and water budgets, and the effects are evident both at local and regional scales. As an example, changes in the Alpine snowpack have influences on the seasonality and amount of the river runoff, and thus on the availability of water in downstream areas during the melting season (Beniston, 2012). Snow cover also affects mountain ecosystems, for example controlling the onset of vegetation growth and the timing of availability of high-quality forage, which is essential for the survival of newborns of selected herbivore species (Mignatti et al., 2012; Pettorelli et al., 2007), as well as the quantity and quality of river water, essential for fluvial organisms (Nilsson and Renöfält, 2008).
Observations from many regions of the world show a decline of snow depth and cover, especially in spring and at locations where air temperatures are close to the freezing point (IPCC, 2013; Brown and Mote, 2009). A shortening of the snow cover duration in spring and a reduction in spring snow depth were found in six high-elevation sites in the European Alps of Switzerland, Austria, and Germany (Marty and Meister, 2012). However, the available information on the past variability of snow resources in mountain areas is far from exhaustive, mainly owing to the paucity of long-term snow observations that are typically sparse and biased toward lower elevation. Currently, the characteristics of the snowpack are still insufficiently monitored owing to the difficulty of establishing and maintaining a dense network of surface stations in high-elevation mountain environments.

The lack of observations can be partially overcome with snow model simulations. Snow models are powerful tools to both estimate the spatial variability of the snowpack and reconstruct the space-time variability of its characteristics in the past. Such simulations rely on the meteorological forcing provided by in-situ stations, or interpolation of ground-based data, or reanalyses. In addition, snow models are employed to estimate future snow changes. In this case, snow schemes can be either nested into global or regional climate models or used off-line and driven by projected meteorological time series provided by climate models (Cassardo et al., 2018a; Cassardo et al., 2018b).

A wide range of snow models has been developed to simulate the temporal evolution of the snowpack characteristics, including snow accumulation, transformation processes, and melting. A distinction can be made between empirical and physical models. Empirical models estimate the solid precipitation fraction and the amount of melted snow through data-based statistical relationships based on temperature and precipitation, which are usually the only two meteorological variables needed as input. These models, even though very simple, can reproduce the snow dynamics with sufficient accuracy using few computational resources. Physical models reproduce the exchange processes between the surface and the atmosphere and they are based on the energy and hydrological balance equations at the Earth's surface. These models can have different degrees of complexity, but they generally require several input variables, such as precipitation, temperature, solar radiation, pressure, humidity, wind direction and wind speed, all at high temporal resolution. For this reason, such models can be quite demanding from the point of view of the required forcings and computing resources. On the other hand, they can take into account many snow processes (such as snow compaction, melting and refreezing water in the snowpack, turbulent and radiation exchanges) and simulate the main snow-related variables (snow density, water equivalent, and snow temperature at various depths).

The choice of the model scheme mainly depends on the specific purpose, the availability of observational and computational resources. Empirical snow models are employed when a coarse estimate of snow depth is sufficient. Physical, but still rather simple snow models are used in complex modelling chain, i.e. in numerical weather prediction systems and in earth system models, to limit the computational costs. Sophisticated multi-layer, physically-based snow models are typically used to reconstruct the vertical structure of the snowpack with a high level of detail and high accuracy.

Commonly, reliable modelling of snowpack evolution in mountain regions is complicated by the high spatial and temporal variability of the meteorological forcings, entailing that surface observations at a given location are scarcely representative of the average conditions of the surrounding area. In this context, it should be underlined that the precipitation input is certainly the main source of error for snowpack simulations in mountains, with strong impacts on model output. It is known that over 1500 m a.s.l. the precipitation measurements, in addition to being rare, are strongly underestimated, especially in winter and in presence of wind (e.g., Frei et al., 2003). For this reason, at international level, various initiatives and experiments are underway to improve the estimation and correction of this parameter (e.g., SPICE, 2012; Harmosnow, 2014).

A recent review paper on the European mountain cryosphere (Beniston et al., 2018) highlighted the major challenges for the snow modelling research. At the catchment scale, i.e. the scale relevant for hydrological applications, a major challenge is to distinguish between the uncertainties introduced by the model structure and those related to the meteorological input data. At regional spatial scales, relevant for weather and climate simulations, large-scale weather and climate models use relatively simple, parametric snow schemes, as these require only a small set of input variables and are computationally less expensive. In this context, future research should aim to clarify the degree of complexity required in snow schemes when integrated in large-scale climate models.

The NextData project contributed to address these research questions with a modelling experiment, NextSnow, which gathered 4 different research institutions (CNR-ISAC, University of Torino, ARPA Valle d'Aosta and CIMA Research Foundation) running six different snow models with different degrees of complexity. This ensemble of models (described in Table 3) includes two sophisticated multilayer snow models (SNOWPACK, Bartelt and Lehning, 2002; and GEOtop Endrizzi et al., 2014), three intermediate complexity physical models (CHTESSEL, Balsamo et al., 2011; UTOPIA, Cassardo, 2015; and SMASH, Piazzi et al., 2018), and a simple empirical model (S3M, Boni et al., 2010). The ensemble thus spans the whole range of model complexities.

Snow Model	# snow layers	Description of the model in a nutshell	Reference
SNOWPACK	Multi-layer	Detailed description of the mass and energy exchange between the snow, the atmosphere, and the soil. Representation of the snowpack microstructure, the internal phase changes and water transport in snow	Bartelt and Lehning (2002)
GeoTOP	Multi-layer	GEOtop describes (i) the heat transfer from atmosphere to soil through the snowpack, (ii) the snow densification (destructive metamorphism and overburden), (iii) the water percolation, and (iv) the accumulation	Endrizzi et al., 2014
CHTESSEL	Single layer	CHTESSEL is energy- and mass-balance model, representing snow liquid water content as a diagnostic; it has a physically based formulation of snow density, revised snow cover fraction and forest albedo in presence of snow	Balsamo et al., 2011
UTOPIA	Single layer	UTOPIA is a third-generation land surface model able to calculate the snow mass, thermal and hydrological balances. It can simulate snow water equivalent, snow water content, snow density, snow depth, snow cover and snow temperature	Cassardo et al., 2015
SMASH	Multi-layer	SMASH is an energy- and mass-balance snow model. It simulates (i) heat exchanges between snowpack, atmosphere, and soil, (ii) sensible and latent heat fluxes, (iii) physically-based evolution of snow density (iv) albedo dynamics. The model supplies predictions of SWE, snow density, snow depth and temperature of each layer.	Piazzi et al., 2018
S3M	Single-layer	Single-layer energy balance snow model designed for hydrological purposes. It combines several sources of information to provide the best estimation of snowpack state.	Boni et al., 2010

Table 3. *Snow models included in the NextSnow experiment.*

The first research question highlighted by Beniston (2018), namely "to better distinguish between the uncertainties introduced by the model structure and the uncertainties related to the meteorological input "data" can be addressed, in principle, by reducing as much as possible the uncertainty in the meteorological input data used to drive snow models. This approach would allow to consider that, the error associated to the model output, is mostly ascribable to the model scheme, while neglecting the error associated to input data. In this context, the NextSnow experiment exploits the uniqueness of the meteorological and snow dataset made available within the NextData project for the experimental measurement site of Torgnon (45°50' N; 7°34'E) at 2160 m a.s.l., located in the mountains of Aosta Valley, in the North-Western Italian Alps (see Figure 5). Torgnon is representative of the high mountain Alpine climate: during the cold season most of precipitation falls as snow and, on average, from the end of October to late May, the site is snow covered with snow depths reaching 90-120 cm. For this site, in the framework of the NextData project, a comprehensive dataset has been collected, with all the variables needed as input by a snow model, i.e. air temperature, total precipitation, wind direction and speed, relative humidity, surface pressure, shortwave and longwave incoming radiation, at high frequency and with a high degree of accuracy. In particular, this site is equipped with the OTT Pluvio2 precipitation gauge, which is able to capture solid precipitation better than standard rain gauges, and thus it allows to reduce the uncertainty on the precipitation input to the snow models. The Torgnon station provides also snow depth, snow density and soil temperatures at different depths, as well as radiation fluxes, whose variables are useful for an in-depth validation of the snow model outputs.

Figure 5. *Torgnon measurement site (45°50' N; 7°34'E) located at 2160 m a.s.l. in the mountains of the Aosta Valley, in the North-Western Italian Alps.*

The accurate and quality controlled meteorological measurements at the Torgnon sites have been used as input to the 6 snow models of the NextSnow experiment to simulate the snowpack conditions between September 2012 and June 2017. The models have been used in their standard configurations, without any calibration, in order to keep these tests as general as possible. An example of the model outputs is displayed in Figure 6 that shows, for each model, the simulated snow depth at Torgnon in the snow season 2012-2013, compared to the observed snow depth. This analysis allows to evaluate each model when it operates under "optimal conditions", i.e. when all the needed inputs are accurately measured (Exp1, Table 4). In these "optimal" conditions SNOWPACK and UTOPIA models, characterized by high and intermediate degrees of complexity, respectively, show the highest agreement with observations. GEOTOP correctly reproduces the observations in winter but it shows discrepancies during the spring season: the snow melting occurs too rapidly and causes the underestimation of the snow peak up to May, when the melting is too slow, resulting in a delayed transition between snow-covered and snow-free condition. CHTESSEL underestimates snow depth during a relevant part of the snow season, from January to April, while it correctly reproduces the snowfall-snowmelt dynamics in the late snow season (May). SMASH underestimates snow depth in the accumulation period, mainly due to a too fast snow settling and the underestimation of some significant snowfall events. The overestimation affecting the model simulations during the melting season, results into a slight delay of the melt-out date. The model S3M, characterized by a low degree of complexity, reproduces well the snow dynamics from the snow onset up to midwinter, while afterwards it shows large discrepancies with respect to the observations. A common feature of most models is the difficulty in the representation of late spring melting, which is often too slow and results in an overestimation of the snow depth (Essery et al., 2013). Only the most sophisticated model, SNOWPACK, which takes into account the snowpack microstructure, is able to correctly simulate late spring dynamics. Among the intermediate-complexity models, UTOPIA shows a good agreement with observations throughout the season and it correctly reproduces the date of snow ablation, i.e. the transition from snow-cover to snow-free conditions.

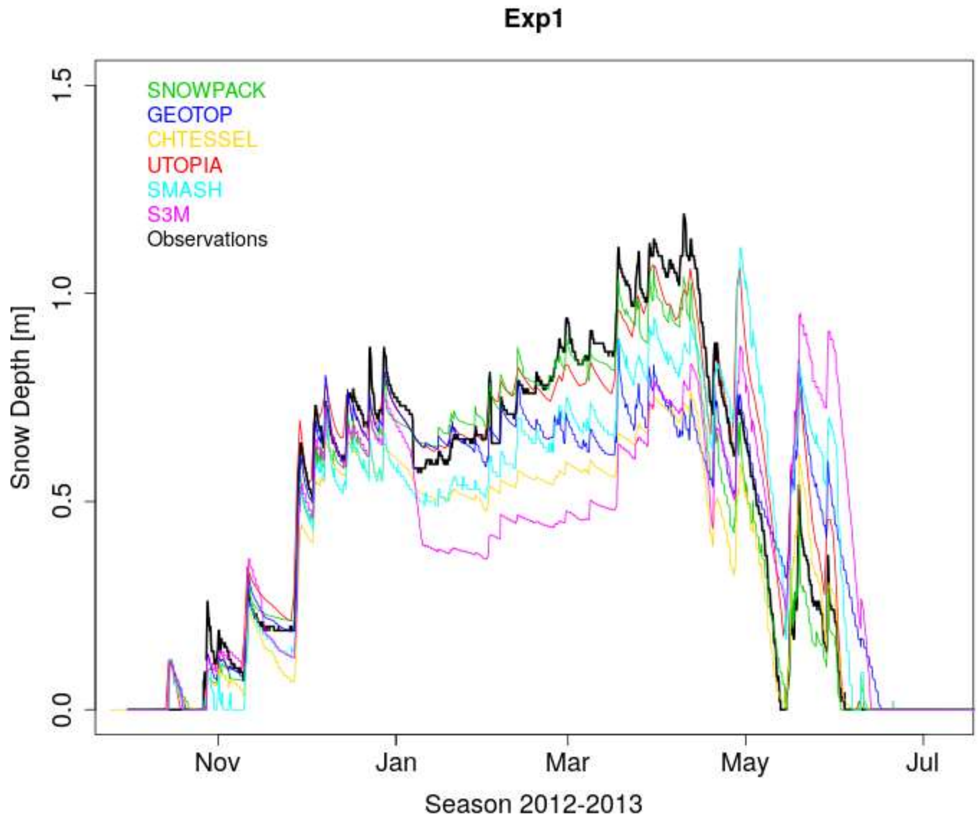

Figure 6. *Simulations of snow depth at Torgnon for each of the 6 snow models, for the snow season 2012-2013. The models are compared under "optimal conditions", i.e. with high quality meteorological forcing.*

As already discussed, the availability of a high-quality meteorological dataset to perform snow simulations is quite uncommon. Standard meteorological stations are typically not able to detect solid precipitation, so they usually significantly underestimate the total amount, especially in mountain areas. Sensors measuring relevant variables, such as incoming shortwave and longwave radiations might be unavailable at most stations, so these quantities have to be parameterized; where no surface station is present, the meteorological forcings have to be estimated through interpolation of the data from the neighbouring stations, or extrapolated from reanalyses. Nevertheless, to which extent the use of lower accuracy input data (from either parameterizations, interpolation of neighbouring stations or reanalyses) affect the performances of the snow models is still an open question. To investigate the impact of the uncertainty in the meteorological forcing on the snow simulations, a set of twelve experiments has been performed (Table 4). These experiments aim to quantify the performance of the snow models when they are forced by: *i)* measured variables except for incoming shortwave radiation, which is estimated from ERA-Interim in case of snowfall (Exp2, Table 4) or parameterized (Exp3); *ii)* drivers with gradually lower temporal resolution, from 30 min down to 12 hours (Exp1, Exp4, Exp5, Exp6); *iii)* drivers derived by spatial interpolation of the nearest surface station measurements (MeteoIO; Bavay and Egger, 2014; Exp7); *iv)* drivers provided by coarse-scale gridded data sets (GLDAS2.1; Rodell et al., 2004; Rui and Beaudoing, 2018; Exp8); *v)* drivers provided by global reanalyses, such as the latest ECMWF product ERA5 (Hersbach and Dee, 2016), at spatial resolutions of 30 km and temporal resolution of 1 hour (Exp9) and the ERA-Interim reanalysis (Dee et al., 2011), at spatial resolutions of 80 km and temporal resolution of 3 hours (Exp10). Further experiments (Exp11 and Exp12) aim to test the effectiveness of bias correction of low-accuracy reanalysis input (ERA-Interim) on the performances of the snow models. All snow model simulations are evaluated in terms of Root Mean Squared Error (RMSE) and BIAS with respect to the observed snow depth.

Exp	Forcing	Time res.	Gap-filling
1	Torgnon station data	30'	ERAI-raw
2	Station data, SWIN, LWIN in case of snowfall are derived from ERA-Interim	30'	ERAI-raw
3	Torgnon station data except for SWIN, Clearsky parameterization	30'	ERAI-raw
4	Torgnon station data	3h	ERAI-raw
5	Torgnon station data	6h	ERAI-raw
6	Torgnon station data	12h	ERAI-raw
7	Interpolation of nearest-stations (MeteoIO)	1h	unnecessary
8	GLDAS	3h	unnecessary
9	ERA5	1h	unnecessary
10	ERA-Interim	3h	unnecessary
11	ERA-Interim_corrected_quota	3h	unnecessary
12	ERA-Interim_corrected_bias	3h	unnecessary

Table 4. *Overview of the experiments carried out with the 6 snow models of Table 3.*

Figure 7 shows the results of the simulations performed with the UTOPIA model. The experiments Exp4, Exp5 and Exp6 use meteorological input obtained by aggregating the surface station measurements at 3, 6 and 12 hour temporal resolution, respectively, and then linearly interpolating them to the time step of the snow models (30'). The three time series of simulated snow depth (cyan, magenta and orange lines) are compared to the corresponding simulations obtained in the reference run of Exp1 (red line). The simulation performed using 3 hourly data is comparable to the one obtained in the reference run with the 30 minute forcing (Table 3). Poorer results are obtained with the 6 and particularly with the 12 hourly data, this latter affected by severe underestimation of snow depth throughout the snow season. This finding is consistent across most models, as summarized in Table 5.

	Exp1		Exp4		Exp10	
	RMSE [m]	BIAS [m]	RMSE [m]	BIAS [m]	RMSE [m]	BIAS [m]
GEOTOP	0.16	-0.12	0.12	-0.05	0.42	-0.38
UTOPIA	0.09	-0.02	0.10	-0.03	0.15	0.02
CHTESSEL	0.18	-0.12	0.17	-0.12	0.25	-0.19
S3M	0.29	-0.20	0.31	-0.22	0.18	-0.15

Table 5. *Evaluation of the snow model simulations in terms of Root Mean Squared Error (RMSE) and bias with respect to the observed snow depth.*

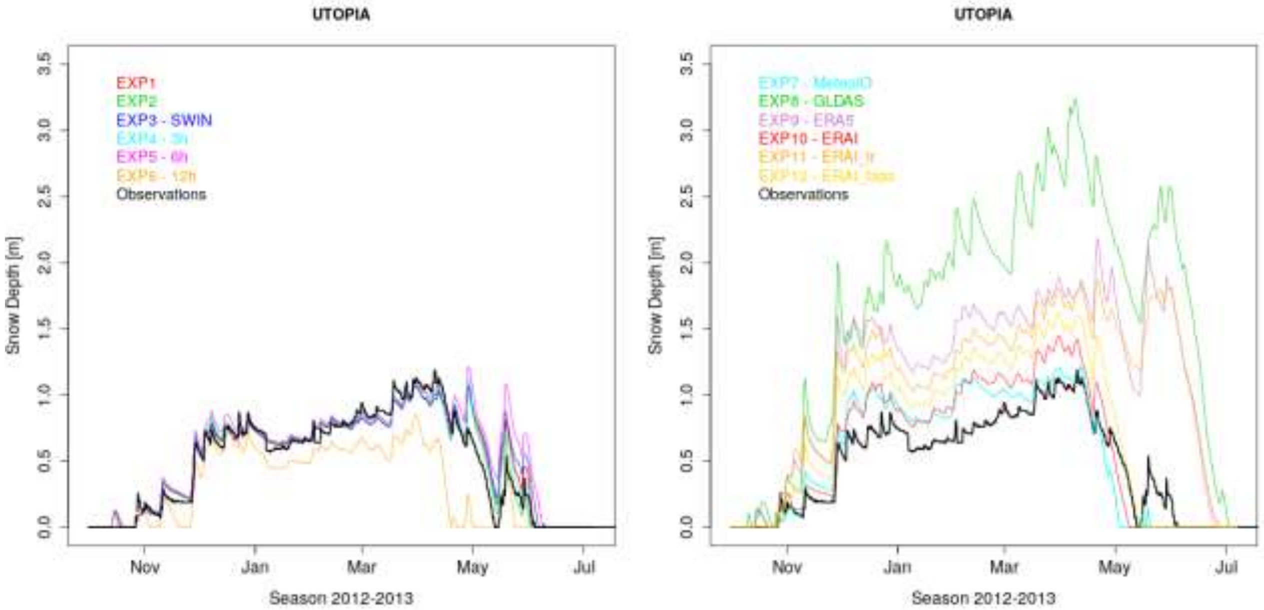

Figure 7. *Snow depth simulations obtained from the UTOPIA model at the Torgnon site (season 2012-2013), for all the 12 Experiments reported in Table 4, compared to the observed snow depth (black line).*

The use of gridded data from interpolation of neighbouring stations measurements as forcing (Exp7) provides a less accurate but still fair reconstruction of the temporal variability of snow depth. The agreement with observed snow depth, of course, depends on the correlations between the meteorological time series at Torgnon and at the neighbouring stations. In specific cases this correlation can be poor, for instance at the end of the snow season (Figure 7, right panel).

Among all simulations forced with reanalyses data (Exp8-Exp12), the better results are obtained with ERA-Interim raw data (Exp10). Despite the coarse spatial (80 km) and temporal (3 hours) resolution of the meteorological forcing, the model is able to reproduce the temporal evolution of snow depth, but with an overall overestimation up to mid-spring, and an earlier snow ablation (Figure 7, right panel).

Large deviations from the observed snow depth are found when the snow models are forced by GLDAS2.1 (Exp8) and ERA5 (Exp9) datasets, mainly due to their biases with respect to the meteorological measurements at the Torgnon site. ERA5, for example, shows a cold and wet bias at the Torgnon gridpoint, with snowfall exceeding more than 50% the observed value. These limitations are consistent with the large overestimation of the snow depth (Figure 7, right panel).

The largest overestimation among all experiments is observed for GLDAS2.1, and an inspection on the input data shows that the main reason for such excess is the overestimation of the precipitation in the input data (with respect to other datasets). Since GLDAS2.1 dataset relies on a mix of meteorological model outputs and (few) observations, the problem is evidently the difficulty of the models used in representing accurately the amount of precipitation.
The analysis presented here, focused on the season 2012-2013, has been extended to the whole period 2012-2017 when the Torgnon data are available to obtain a more robust quantification of the sensitivity of the snow models to the accuracy of forcing data. The complete results are being collected in a paper (in preparation) that addresses the trade-offs between the complexity of snow models and model performances, with the purpose of using the best performing models to simulate past and future condition of mountain snowpack at fine spatial scales.

6.4 Historical climatic time series and daily climatic snow cover dataset

S. Fratianni[1, 2], F. Acquaotta[1, 2]

[1]*University of Torino, Department of Earth Sciences, Torino, Italy*
[2]*University of Torino, Natrisk, Centro Interdipartimentale sui Rischi Naturali in Ambiente Montano e Collinare, Torino, Italy*

6.4.1 Background

The investigation on snow precipitation and snow cover variability is fundamental in the frame of climate change studies and in developing strategies for the mitigation of climate change effects. At local scale, the need of information about snow precipitation amount, duration and variability is required for a correct socio-economic planning, which takes into account the changing environment.
Concerning Italian Alps, the information on winter precipitation variability is still scarce compared to the Swiss, French and Austrian sides. Even though some regional studies have already been produced (Terzago et al., 2012, 2013; Fratianni et al., 2015), this field can be still considered as underexplored due to the difficulty of finding long term and continuous time series.
In the frame of NextSnow project, the effort is then addressed to recover historical climatic time series and enhance a unique and unexplored daily climatic dataset. The data originally reported over bulletins were digitalized, quality controlled, checked for homogeneity and then analysed to investigate trends and variability of snow.

6.4.2 Data

The historical time series used in this study, have been recovered from the paper archives of the Ufficio Idrografico del Bacino del Po (Po Basin Hydrographic Office) operational since 1920's up to 1990 and then merged to the Arpa (Regional Agency for Environmental Protection) of Piemonte, Lombardia, and Valle d’Aosta (Figure 8).


SOCIETÀ EDISON

MINISTERO DEI LAVORI PUBBLICI
UFFICIO IDROGRAFICO DEL GENIO CIVILE
PER GLI STUDI DEL BACINO DEL PO

SERVIZIO DISTACCATO CENTRALE TOCE

TEMPERATURA

Figure 8. *Extract of the paper that were digitalized data and metadata: an example of the Lake Vannino station in February 1954.*

All the measurements are performed manually by the observers with graduated snow stakes and snow tablets (Figure 9).

Figure 9. *Meteorological station of Lago Goillet (Bertolotto et al., 2018).*

The main parameter used in this study is snow depth (HS). In most cases, fresh snow precipitation (HN) observations are not systematically registered, so, in order to have continuous and comparable data, HN is calculated by subtraction of two consecutive HS values. The data finally analysed refer to the 33 manual daily snow height stations covering the whole Italian North-

Western Alps and ranging between 605 and 2526 m a.s.l. (Figure 10). The longest time series supply 91-years records (1925-2015) and the shortest ones 40-years records (1966-2005) and they all almost continuous.

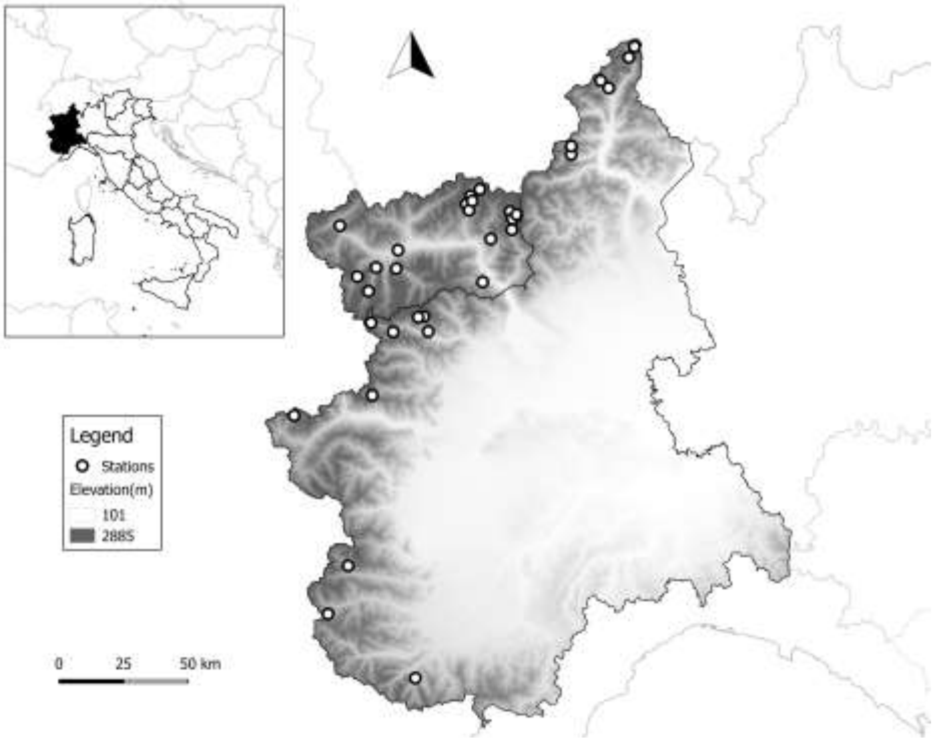

Figure 10. *Geographical position of the stations selected for this study, located in the Piemonte and Valle d'Aosta, NW Italy.*

6.4.3 Methodology

Snow depth and fresh snow data, performed and registered by observers on the bulletins, have been digitalized together with all the notes regarding the measurements or the instruments anomalies.

A parallel in-depth historical research has been carried out in order to acquire stations metadata. Particular attention has been addressed to eventual relocations or changes undergone during the station lifetime, which could reflect the inhomogeneities in the time series and relevant changes in the data not related to climatic factors (Peterson et al., 1998; Aguilar et al., 2003; Acquaotta et al., 2009, 2016).

All the time series have been quality controlled in order to identify, and eventually correct, anomalous values and errors due to the observers or to the process of digitization. Snow height time series have been quality checked using the QCSnow (Quality Control on Snow data, Bertolotto et al., 2018) which highlights unreasonable values.

QCSnow is written in R open source language. The script is divided in 3 steps:

- pre-checks show the incorrect values due to erroneous transcriptions of the daily data. It has 3 conditions: *1)* HN ≥ 0 cm and HS ≥ 0 cm, *2)* HS ≥ HN and *3)* ΔHS between two consecutive days < 30 cm;
- completeness checks statistically characterization of the snow series, HN and HS, and the gaps identification. The mean, median, first and third quartile, the maximum and minimum values are identified. Also, a monthly, seasonally and annual scatter plot are created;

- climatological checks calculate the alert thresholds and highlights the outliers. For every series daily and monthly thresholds are estimated by percentiles, 95p and 99p, and 4*standard deviation.

The suspect values and the outliers are stored in tables and then cross them to highlight common periods so to start the manual and spatial control. The manual control checks the data in the original paper records while the spatial control compares the data with the data of the neighbouring stations.

Daily values have been aggregated over monthly and seasonal time scales. These data have been retained only if at least 80% of the daily values were available (Baronetti et al., 2018; Klein Tank et al., 2002) and then a trend analysis has been performed by least square linear fitting (Zhang et al., 2000). The significance of the trends has been evaluated with the non-parametric Mann-Kendall test, at 95% confidence level (Yue and Wang, 2004; Sneyers, 1990). For each station, the seasonal snow depth standardized anomalies have also been calculated.

6.4.4 Conclusions

The present study gives a contribution to the assessment of the temporal and spatial variability of the climatic conditions at high elevation sites in Western Italian Alps since 1925. In accordance to the NextSnow initiative, several historical daily snow depth time series have been recovered from the paper archives of several Institutions. The time series are representative of all the Western Italian Alps and they allow to explore a range of altitude between 900 and 2300 m a.s.l., spanning at almost 55 years period.

Finally, a new and extensive dataset of high-quality snow data series will be made available. These values can be used in a large area located in the north-western Alps for evaluating the climate changes and the occurrence of extreme events, essential for the proper identification of trends and future scenarios. These datasets are required in order to provide input to extended historical reanalysis (i.e., reanalyses prior to 1948), to calibrate satellite estimates of surface variables, and to provide better observational data for the validation of climate model outputs.

Apart from their scientific value, the NextSnow datasets also offer political, socioeconomic outcomes and are required to: *1)* contribute to advanced identification and understanding of climate change, *2)* improve knowledge on the snow cover variability and the factors that influence it, and *3)* contribute to the contextualization of the results.

6.5 Snow Melt Processes on Mountain Slopes

S. Ferraris[1], Maurizio Previati[1], Davide Canone[1], Davide Gisolo[1], Hendrik Huwald[2]

[1]*Polytechnic and University of Torino, Interuniversity Department of Regional and Urban Studies and Planning, Torino, Italy*
[2]*Ecole Polytechnique Fédérale de Lausanne (EPFL), School of Architecture, Civil and Environmental Engineering, Lausanne, Switzerland*

6.5.1 Review of Energy Balance and Turbulent Fluxes at Inclined Surfaces

The energy and water flux components involved in snowmelt processes are major controls of the alpine water cycle. They are a consequence of local climate and constitute a key control on many strategic topics like winter ecological processes (e.g. Campbell et al., 2005), soil moisture storage through snow melt infiltration and recharge of water bodies (e.g. Hayashi et al., 2003), stream flow (e.g. Jepsen et al., 2012; Brauchli et al., 2017), hydropower production (e.g. Schaefli et al., 2007; Schaefli et al., 2019), and avalanche hazard (e.g. Lehning et al., 2004).
The energy and water fluxes can show strong temporal and spatial variability especially on steep and sun-exposed alpine slopes, where the snow-covered area can vary very quickly in time, with corresponding large albedo variations. In addition, migration of terrain-cast shading on the slope can result in surface temperatures variations of up to 20°C in just a few minutes (Nadeau et al., 2013). Such phenomena are expected to become more relevant with global warming, causing a feedback on air temperatures, with reduced snow-covered areas, lower surface albedo, and increased net radiation (e.g. Diffenbaugh et al., 2005; López-Moreno et al., 2013).
Despite this relevance, observational data from alpine and subalpine slopes are rare, mainly because of the measurement difficulties. Today, eddy covariance (EC) is the most used technique to measure the turbulent fluxes of energy and water vapour in the lowest layer of the atmosphere, but its use in mountain areas is difficult, due to often severe weather conditions, and the complex morphology. The bulk method based on Monin-Obukhov Similarity Theory (MOST) is an alternative method to EC for determining the sensible heat flux (Arck and Scherer, 2002), however, most theoretical assumptions of MOST are not applicable in this type of terrain or require significant adjustments (Oldroyd et al., 2015). In addition, MOST has been shown ineffective in determining plausible values of turbulent fluxes in particular environments such as locally homogeneous forest clearing during the snowmelt season (Helgason & Pomeroy, 2005).
A method for analyzing the scalar turbulent fluxes measured by EC is the computation of the Energy Balance Closure (Wilson et al. 2002; Datt et al., 2008). It requires that the sum of the turbulent heat fluxes equals the sum of all other energy fluxes at the surface plus change in snow internal storage:

$$LE + H = Rn - G - S\,(-A) \qquad (1)$$

where LE and H are the latent and sensible heat flux, respectively, Rn is the net radiation, G is the conductive heat flux into the soil (or the soil in absence of a snow cover) at the level of the sensor, S is the rate of change of thermal energy stored in the layer of soil and in the snow above the heat flux sensor, and A is the rate of change of heat storage (air and biomass) between the soil surface and the level of the EC instrumentation (negligible in most conditions).

Measuring the individual energy balance components and closing the balance based on these observations without significant residuals is experimentally challenging. Aubinet et al. (2000) and Wilson and Baldocchi (2000) have shown that the turbulent fluxes of energy are generally and consistently underestimated. From a number of sites within the "FLUXNET" network it has been found that surface turbulent energy fluxes are frequently underestimated by about 10-30% relative to the measured net radiative energy Rn (Wilson et al., 2002).

Although not very significant, residuals in the energy balance closure were even detected on simple flat surfaces with uniform and low vegetation (Twine et al., 2000). Leuning et al. (2012) state that, although turbulent fluxes of energy are underestimated in most EC sites, a large part of this underestimation can be explained by incorrect estimates of the energy stored in air and biomass below the measurement height.

Concerning the application of the EC method in highly complex terrain, there are some results of studies conducted in slope conditions. Hammerle et al. (2007) analyzed the energy balance during the growing season at two grassland sites in the Alps. One site was on a slope with an average inclination of 24° and exposed to northeast, the other was situated on a flat terrain. They concluded that EC measurements made above the slope were of similar quality as fluxes measured over the flat terrain. Hiller et al. (2008) measured turbulent heat and CO_2 fluxes using the EC method on a slope with an inclination of 25° in the Swiss Alps. Although they could not find any indication that the EC method does not work on complex terrain, they proposed a more sophisticated study with more EC towers in order to fully confirm their findings. To investigate slope flows and small-scale dynamics occurring close to the surface (namely the evening transition of slope flows on clear-sky summer days), Nadeau et al. (2013) deployed two turbulence towers (single and multi-leveled measurement) and several meteorological stations (two weather stations, five surface temperature measurement stations and a tethered balloon system) along a transect on a steep west facing mountain slope in the Swiss Alps from 1900 to 2200 m a.s.l. They found that the timing and the dynamics of the evening transition of slope flows (from convective to katabatic) is mostly controlled by the local radiation balance.

Saitoh et al. (2011) evaluated the closure of energy balance over a temperate forest on a 21° steep slope in a snowfall-dominated region over a three-year period. Their experimental site had a north-northeast aspect, with monthly average winter temperatures in a range of about 3-5°C, annual mean air temperature of 10.6°C, and annual mean precipitation of 1738 mm. They concluded that the energy balance closure at the slope site was of similar degree of accuracy as those over a flat topography.

With reference to snow-covered ground, the EC technique has been used in terrains of varying complexity. The first applications over snow were conducted at homogeneous sites such as frozen lakes or flat glaciers (e.g. Hicks and Martin, 1972; Andreas et al., 1979). Some studies have focused on the sublimation of the snowpack and the effects that the vegetative cover may have on it (e.g. Nakai et al. 1999; Reba et al., 2009; Reba et al., 2011), while others investigated the interaction between vegetation and soil (e.g. Turnipseed et al., 2003), and also surface hoar dynamics (Stossel et al., 2010). Mott et al. (2013) evaluated the micrometeorological processes related to the snow ablation in an Alpine catchment and they found that radiation dominates the snow ablation early in the season, while the advection contribution becomes important late in the season, and they

assumed the existence of a stable boundary layer above a patchy snow cover that exerts a dominant control on the timing and magnitude of snow ablation.
Few studies analyzed the closure of the energy balance at a snow-covered site. Reba et al. (2009) collected three years of observations at a wind-exposed mountain site with mainly sagebrush vegetation. Differently from the present study, it was not located on a slope. They concluded that this application of EC was viable, conditionally on performing corrections and postprocessing, including wind filtering, double rotation and tilt correction. Chen et al. (2011) studied the energy balance partitioning before, during and after the snowfalls on a flat meadow in Eastern Mongolia and they concluded that a diurnal cycle existed in the energy balance: a diurnal partitioning of incident energy Rn into LE in the snow-melted phase, and into H in the snow-melting phase. Helgason and Pomeroy (2012) investigated the internal energy evolution of snow-cover during a snow melting period and they found large imbalances in measured energy caused by longwave radiation losses that were not compensated by downward turbulent fluxes, solar radiation or conductive heat from the ground. Finally, Mott et al. (2017) investigated with the EC technique the heat fluxes over melting snow in complex Alpine terrain. Their results highlight the boundary layer characteristics: when the snow cover is continuous, the boundary layer above is stable and the downward turbulent heat fluxes are small. Instead, the boundary layer is unstable for a patchy snow cover. They conclude that simple parameterization of subgrid snow cover fractions and applying simple gradient–flux relationships at the same time in regional atmospheric models may lead to large biases in flux estimates.
The objective of the experimental study presented in the following, is to measure energy and mass fluxes during rapid snowpack melting events.

6.5.2 Cogne Test Site Case Study Results

This section presents measurements on a steep slope with east-south-east aspect in alpine environment using an EC station. Due to its exposition, the slope is subject to rapid transitions from snow-covered to snow-free conditions, and large variations in albedo, surface temperature and soil water content, even in winter.
The study was carried out on a slope near the town of Cogne in the North-Western Italian Alps at 1730 m a.s.l. on a 26° steep slope facing east-south-east (120°). The vegetation is characterized by herbaceous and shrub components typical of degraded pastures at high altitudes, representative of wide areas in the Alps. Precipitation occurs mainly in spring and autumn, with an annual mean of 646 mm per year (for the 1996 to 2016 period), with on average 87 days per year with precipitation larger than 1 mm. The average annual temperature is about 4°C.
The test site was equipped with a three-dimensional sonic anemometer (Campbell Sci., CSAT3), a Vaisala HMP45C air temperature and relative humidity probe, and an open path infrared gas analyzer (Licor, Li-7500A), at a vertical height of 2.10 m above the surface. Data were sampled at a frequency of 10 Hz, then averaged over a 30 min period. The following sensors were set up additionally: *i)* a Kipp&Zonen NR-LITE net radiometer, *ii)* a Campbell Sci. CS616 probe for the measurement of water content using Time Domain Reflectometry (TDR), *iii)* two Campbell Sci. TCAV thermocouples for the measurement of the soil temperature, *iv)* two Hukseflux HFP01SC soil

heat flux plates for the measurement of conductive heat fluxes within the soil, and *v)* an Apogee Instruments IRTS-P infrared sensor for the measurement of the surface temperature.
As soon as a snowpack develops on the ground, it interacts with the atmosphere, and with the soil interfaces. According to theory, the system input and output quantities should be balanced. To investigate the complex morphology effect, the test site was selected excluding canopy interception (and canopy interactions), and relevant wind transport phenomena, therefore, observed changes and conditions are expected to result from energy exchange only.
An autumn event is presented in Figure 11. It is interesting that the fast melt dynamics occur also in a season when the solar radiation is relatively low. Panel (d) shows the snow water equivalent (in blue) and the evolution of soil water in the following days. The red line represents the amount of sublimated and evaporated water, roughly proportional to the energy deficit in the balance equation. It is evident that most snow melts during the first day, despite low net radiation compared to the next days (no melting was detected during the snowfall). The following days are characterized by larger net radiation, resulting in emerging patches of soil, consequently leading to progressively increasing sensible heat flux and soil surface temperature. In addition, the evolution of the soil water content emphasizes the persistence of patchy snow that melts in the following days. During the melting period, the topsoil temperature remains always above freezing, while the soil surface infrared temperature and the air temperature oscillate between freezing (night-time) and melting (day-time) conditions. Finally, wind speed remains always modest, mostly related to diurnal upslope breezes and nocturnal katabatic wind.
Regarding the energy balance, the obtained closure is quite satisfactory, and comparable to the results in Reba et al. (2009). The patchy snow cover causes the increase in the sensible heat flux (grey line), even before all the snow has melted. Finally, as soon as the snow cover fully disappears, the soil heat flux increases notably, as a result of the sharp drop of surface albedo. Also, the latent heat flux follows the diurnal cycle with peaks during the day as a result of intense evaporation and sublimation. Additional energy to the system can be provided by the energy stored in soil. However, this interaction is not very evident: on the one hand, the snowpack constitutes a real insulating layer preventing the soil to absorb more energy; on the other hand, the presence of a discontinuity in the snow-soil contact can strongly reduce any exchange flux. This discontinuity is usually caused by physical obstacles (e.g. residues of vegetation), but in normal conditions, the processes of melting and refreezing can lead to similar discontinuities (e.g. depth hoar growth). The above mentioned insulation layer may be dynamic in time and space because the residual vegetation layer evolves, from autumn to spring, modifying its shape due to compression by over lying snow, and biological degradation, therefore in autumn the layer of insulating air is larger and more effective than in spring. Furthermore, once the snowmelt process exposes some portions of soil surface, local boundary layers circulation effects at the edges of snow patches further accelerate the snowmelt processes (Mott et al., 2013).

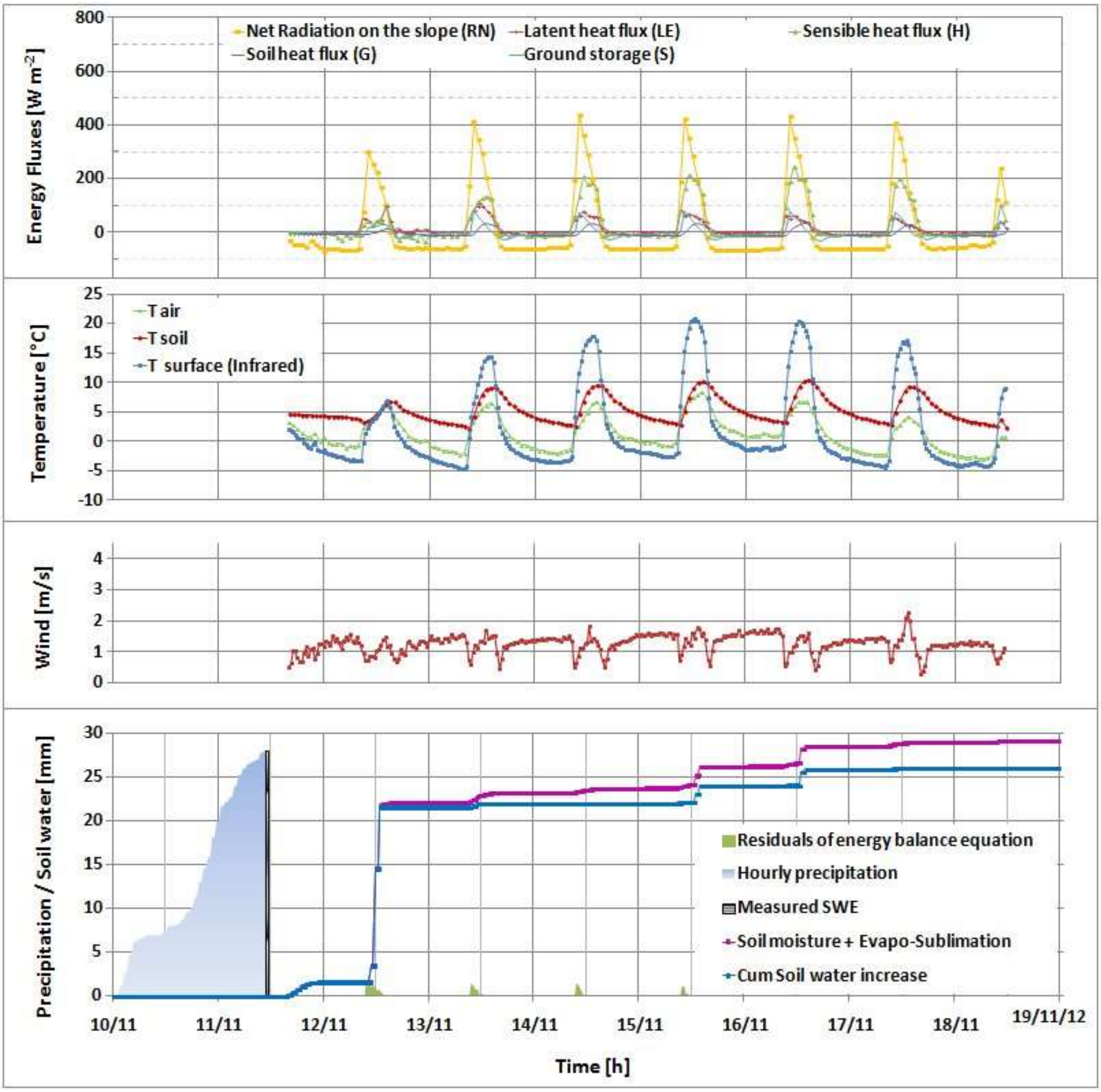

***Figure 11**. (a) Surface energy balance flux components, (b) air, surface and soil temperature, (c) wind speed, and (d) cumulated hourly precipitation and snow water equivalent at the Cogne test site during an autumn fast snowmelt event (November 10th to 19th, 2012). The blue line in d) is the increase (mm) of soil moisture, while the red line is the sum of that increase and the calculated loss of water (mm) through evaporation and sublimation of snow.*

6.5.3 Conclusions

The physics of rapid snowmelt events on vegetated slopes is quite complex, and further research needs to be done. As a preliminary result, a quite close balance of mass was obtained during the melting transient. Regarding the energy balance, a better closure is obtained keeping into account the melting related terms, but some more uncertainty is present, in comparison with the mass balance. The observed nonlinearities suggest possible relevant effects also at the regional scale simulations. In a next step, the mass and energy balance components measurements will be compared to corresponding model simulations at the local scale, using a detailed physical snow cover model, e.g. SNOWPACK (Lehning et al., 2004).

6.6 Snow water equivalent in the Alps as seen by gridded datasets, CMIP5 and CORDEX climate models

S. Terzago[1], E. Palazzi[1], J. Von Hardenberg[1], A. Provenzale[2]

[1]*CNR-ISAC, National Research Council of Italy, Institute of Atmospheric Sciences and Climate, Torino, Italy*
[2]*CNR-IGG, National Research Council of Italy, Institute of Geosciences and Earth Resources, Pisa, Italy*

In a context of climate change, reliable regional estimates of past and future expected changes in snow cover, are essential to develop adaptation and management strategies. Detailed studies on the recent and projected impacts of global warming in snow-dominated regions are necessary to inform future management of water resources and to preserve essential ecosystem services for millions of people living in downstream areas. As seen in the previous paragraphs, the density of surface stations measuring snow is currently insufficient to develop a reliable gridded snow water equivalent dataset based on in-situ measurements, thus calling for the use of alternative sources of information on snow depth and mass, derived from remote sensing observations and reanalyses (Mudryk et al., 2015).

Satellite measurements have been shown to provide a reliable picture of the global snow cover extent at few hundred meters spatial resolution (Brown et al., 2010; Hall and Riggs, 2007), while the estimation of snow depth and snow water equivalent from satellite, is typically performed at spatial scales of 25 km and it is more challenging (Salzmann et al., 2014). Global reanalyses provide snow water equivalent fields at horizontal resolutions that are comparable (30 km in the zonal direction) or coarser than satellite products. Some reanalyses, such as ERA-Interim (Dee et al., 2011) and NCEP-CFSR (Saha et al., 2010), assimilate surface snow depth measurements and satellite snow cover extent while others, such as MERRA (Rienecker et al., 2011) and 20CR (Compo et al., 2011), are not constrained by measurements and thus rely on the capability of their land-surface model component to estimate snow fields.

To date, few studies have investigated the accuracy of satellite-based and reanalysis snow water equivalent (SNW) datasets against available observations, and very little is known on their performances in mountain areas. In the present study, first, we review the available snow water equivalent (SNW) datasets and quantitatively assess the uncertainties in the estimation of the snow water equivalent in the Alpine environment. We consider global SNW gridded datasets obtained from satellite and reanalysis data and we explore how they represent the snow climatology over the Greater Alpine Region (GAR, 4–19°E, 43–49°N). Based on this analysis, we discuss the performances of state-of-the-art SNW products in this orographically complex area and we provide an estimate of the inter-dataset spread in the Alps. Second, these results are used as a reference for evaluating the state-of-the-art climate models participating in the two major coordinated experiments: CMIP5, providing global simulations at average spatial resolution on the order of 100 km, and EURO-CORDEX providing regional simulations up to 12 km spatial resolution over the European domain. For each of the 36 GCMs and 5 RCMs listed in Table 6 and Table 7 respectively, we assess the ability to represent: *(i)* the main drivers of snow processes, i.e. surface air temperature and precipitation, compared to the observational dataset EOBS (Haylock et al., 2008), and *(ii)* the snow water equivalent climatology compared to the ensemble mean of the reference satellite and reanalysis datasets.

Model	Institution	LSM	Res. [lon]/Sp.Res	Reference
NSIDC-SNW	National Snow and Ice Data Center	–	25 km	Armstrong et al. (2005)
AMSR-E	National Snow and Ice Data Center	–	25 km	Tedesco et al. (2004)
CFSR	US National Centers for Environmental Prediction	Noah	0.3125	Saha et al. (2010)
MERRA	US National Aeronautics and Space Administration	Catchment LSM	0.67	Rienecker et al. (2011)
ERA-Interim/Land	European Centre for Medium-Range Weather Forecasts	HTESSEL	0.7	Balsamo et al. (2013)
20th Century Reanalysis	NOAA Earth System Research Laboratory	Noah	1.875	Compo et al. (2011)
CMCC-CM	Euro-Mediterranean Centre for Climate Change	ECHAM5	**0.75**/T159	Scoccimarro et al. (2011)
EC-Earth	EC-Earth Consortium	HTESSEL	**1.125**/T159	Hazeleger et al. (2012)
BCC-CSM1-1-M	Beijing Climate Center, China	BCC_AVIM1.0	**1.125**/T106	Wu et al. (2013)
MRI-CGCM3	Meteorological Research Institute, Japan	HAL	**1.125**/T159	Yukimoto et al. (2012)
CESM1-BGC	National Center for Atmospheric Research	CLM4	**1.25**	Hurrell et al. (2013)
CESM1-CAM5	National Center for Atmospheric Research	CLM4	**1.25**	Hurrell et al. (2013)
CESM1-FASTCHEM	National Center for Atmospheric Research	CLM4	**1.25**	Hurrell et al. (2013)
CCSM4	National Center for Atmospheric Research	CLM4	**1.25**	Gent et al. (2011)
CNRM-CM5	Centre National de Recherches Météorologiques	ISBA	1.4/T127	Voldoire et al. (2013)
ACCESS1-0	CSIRO/BOM, Australia	MOSES2	1.875/N96	Bi et al. (2013)
ACCESS1-3	CSIRO/BOM, Australia	CABLE1.0	1.875/N96	Bi et al. (2013)
CMCC-CMS	Euro-Mediterranean Centre for Climate Change	ECHAM5	1.875/T63	Scoccimarro et al. (2011)
CSIRO-Mk3-6-0	CSIRO, Australia	MOSES II	1.875/T63	Collier et al. (2011)
HadGEM2-AO	Met Office Hadley Centre	MOSES II	1.875/N96	Collins et al. (2011)
HadGEM2-CC	Met Office Hadley Centre	MOSES II	1.875/N96	Collins et al. (2011)
HadGEM2-ES	Met Office Hadley Centre	MOSES II	1.875/N96	Collins et al. (2011)
MPI-ESM-LR	Max Planck Institute for Meteorology	JSBACH	1.875/T63	Giorgetta et al. (2013)
MPI-ESM-MR	Max Planck Institute for Meteorology	JSBACH	1.875/T63	Giorgetta et al. (2013)
MPI-ESM-P	Max Planck Institute for Meteorology	JSBACH	1.875/T63	Giorgetta et al. (2013)
INM-CM4	Institute for Numerical Mathematics	INM	2.0	Volodin et al. (2010)
CESM1-WACCM	National Center for Atmospheric Research	CAM	2.5	Hurrell et al. (2013)
GFDL-CM3	NOAA Geophysical Fluid Dynamics Laboratory	LM3	2.5	Donner et al. (2011)
GFDL-ESM2G	NOAA Geophysical Fluid Dynamics Laboratory	LM3	2.5	Dunne et al. (2012)
GFDL-ESM2M	NOAA Geophysical Fluid Dynamics Laboratory	LM3	2.5	Dunne et al. (2012)
GFDL-CM2p1	NOAA Geophysical Fluid Dynamics Laboratory	LM2	2.5	Delworth et al. (2006)
GISS-E2-H-CC	NASA Goddard Institute for Space Studies	GISS LSM	2.5	Schmidt et al. (2006)
GISS-E2-H	NASA Goddard Institute for Space Studies	GISS LSM	2.5	Schmidt et al. (2006)
GISS-E2-R-CC	NASA Goddard Institute for Space Studies	GISS LSM	2.5	Schmidt et al. (2006)
GISS-E2-R	NASA Goddard Institute for Space Studies	GISS LSM	2.5	Schmidt et al. (2006)
NorESM1-ME	Norwegian Climate Centre	CLM4	2.5	Bentsen et al. (2013)
NorESM1-M	Norwegian Climate Centre	CLM4	2.5	Bentsen et al. (2013)
BNU-ESM	Beijing Normal University, China	BNU-CoLM3	2.8125/T42	*
CanESM2	Canadian Centre for Climate Modelling and Analysis	CLASS	2.8125/T63	Arora et al. (2011)
FGOALS-g2	LASG/CESS, China	CLM3	2.8125	Li et al. (2013)
FIO-ESM	The First Institute of Oceanography, China	CLM3.5	2.8125/T42	Qiao et al. (2013)
HadCM3	Met Office Hadley Centre	MOSES I	3.75/N48	Johns et al. (2003)

* Reference is http://esg.bnu.edu.cn/BNU_ESM_webs/htmls/index.html.

Table 6. *Snow water equivalent data sets, including remote sensing products, reanalyses and CMIP5 global climate models used in the study, with the corresponding land-surface model (LSM, when it applies) and the spatial/spectral horizontal resolution (from Terzago et al., 2017).*

Model	Institution	LSM	Ensemble members	Reference
CCLM4-8-17	CLM Community	Terra-ML	4	Rockel et al. (2008)
ALADIN53	Centre National de Recherches Météorologiques	ISBA	–	Farda et al. (2010)
HIRHAM5	Danish Meteorological Institute	Hagemann (2002)	1	Christensen et al. (2007)
RACMO22E	Royal Netherlands Meteorological Institute	HTESSEL	2	Van Meijgaard et al. (2012)
REMO2009	Climate Service Center	Hagemann (2002)	1	Jacob and Podzun (1997)

Table 7. *EURO-CORDEX regional climate models providing ERA-Interim-driven runs for the snow water equivalent variable at 0.11◦ spatial resolution considered in this study. For each of model we also report the land-surface model (LSM), the number of available GCM-driven runs and the reference.*

The results of the analysis show that the time-averaged spatial distribution (Figure 12) and amplitude of the snow water equivalent annual cycle (Figure 13) are reproduced quite differently by the different remote sensing and reanalysis datasets, which in fact exhibit a large spread around the ensemble mean. The information on snow water equivalent climatology provided by these datasets is affected by large uncertainties, thus it can be considered only qualitatively.

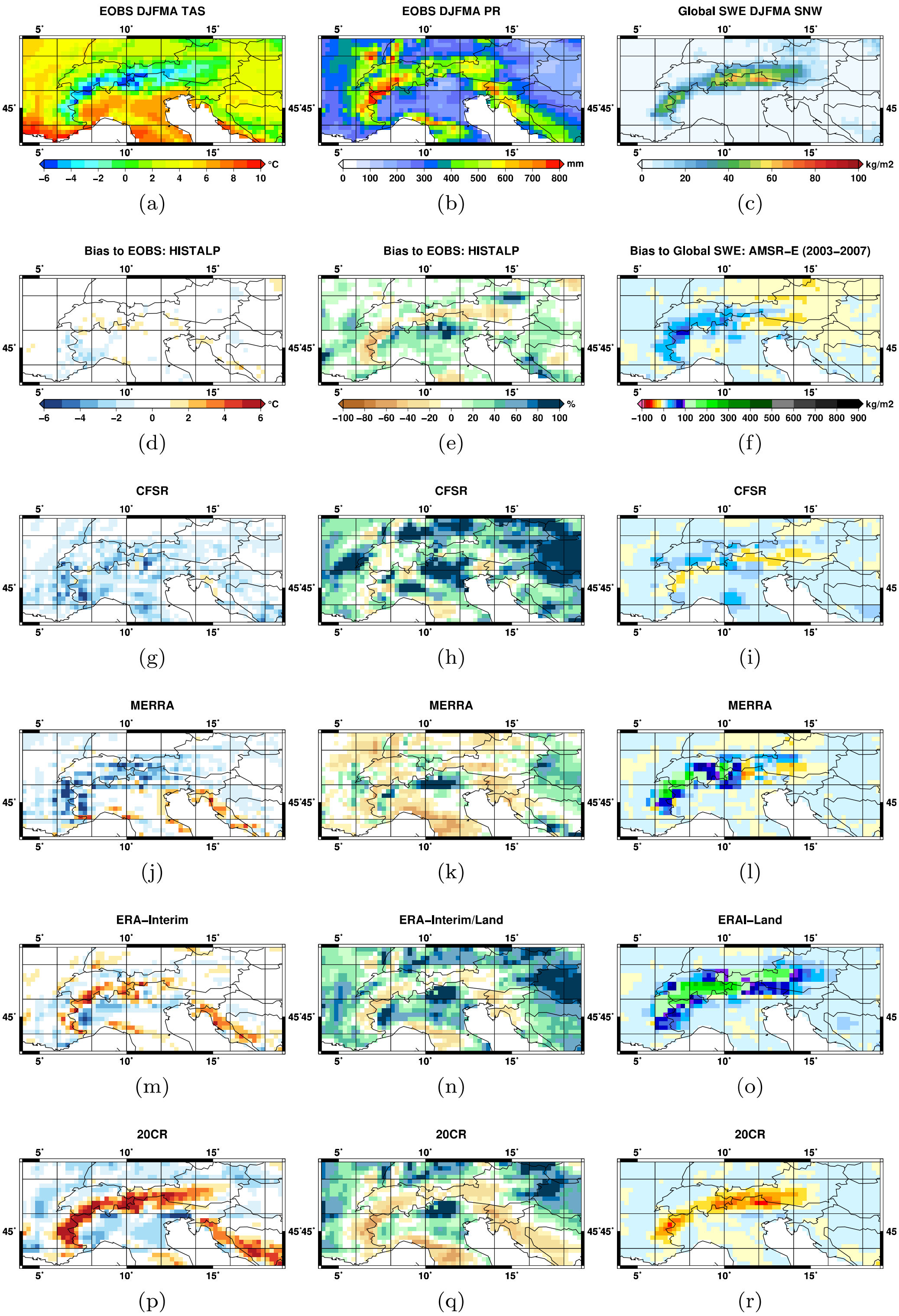

Figure 12. *Multiannual mean (1980–2005) of the DJFMA average (a) air temperature, (b) total precipitation from EOBS observational datasets and (c) snow water equivalent from NSIDC-SNW. Panels from (d) to (r) represent the bias of HISTALP, AMSR-E and reanalyses with respect to EOBS and NSIDC-SNW data sets respectively (from Terzago et al., 2017).*

Regarding global climate models, GCMs with spatial resolutions finer than 1.25° longitude (hereafter defined as "high resolution GCMs") are in closer agreement with the ensemble mean of satellite and reanalysis products in terms of root mean square error and standard deviation than lower resolution GCMs. Still, one should take into account that all GCMs have evident limitations in representing the distribution of altitudes in the greater Alpine region, with the most resolved models underestimating the 95th percentile of the distribution by 500-800 meters. GCMs do not take into proper account elevations above 1500-2000 m a.s.l., which are simply non-represented in most models.

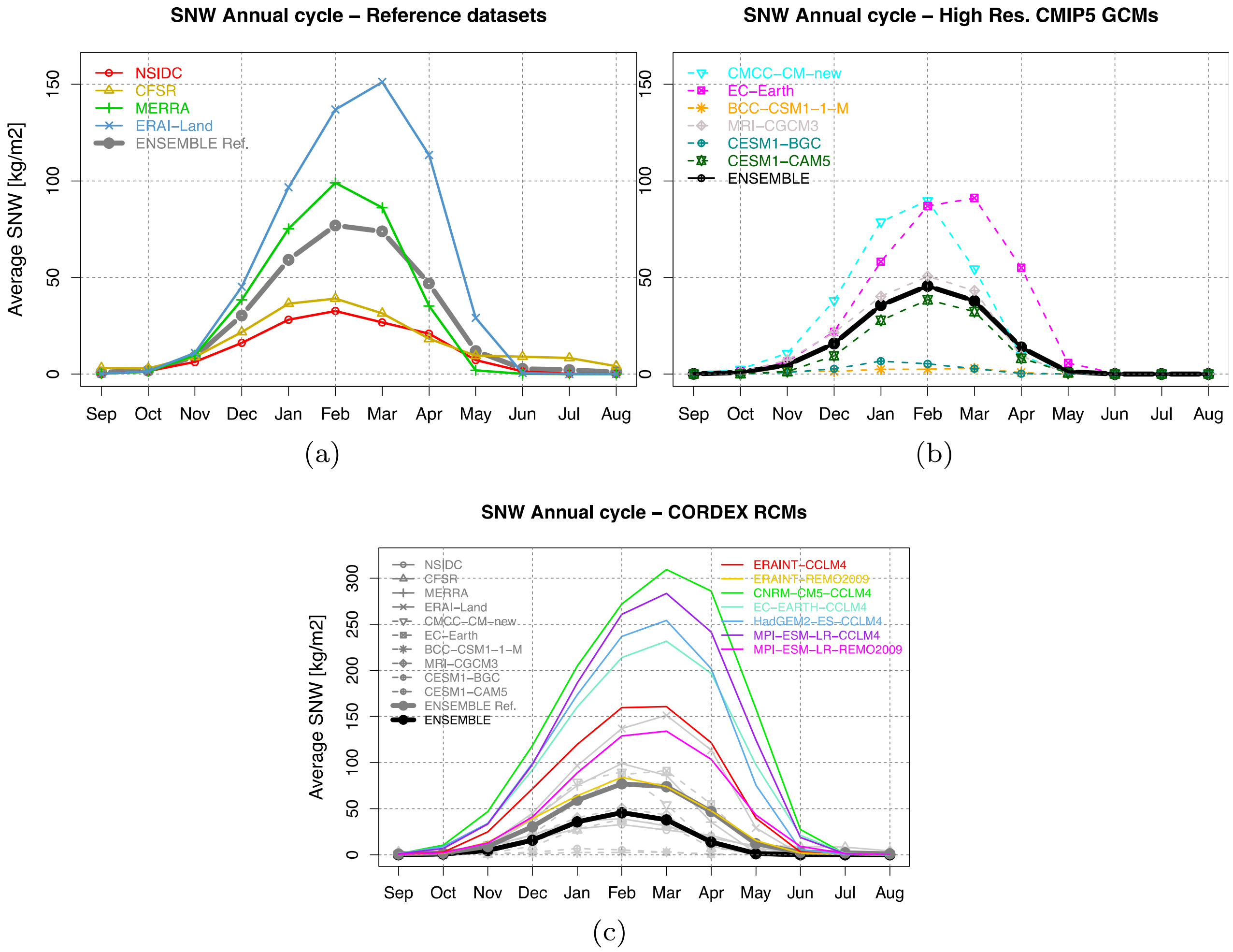

Figure 13. *(a) Annual cycle of snow water equivalent in the reference data sets and (b) in CMIP5 high-resolution GCMs (spatial averages over areas above 1000 m a.s.l., temporal averages over the historical period 1980–2005). (c) Annual cycle in ERA-Interim-driven and GCM-driven regional climate model simulations, calculated over the period 1990–2005, in comparison to reference data sets and GCM simulations.*

The EURO-CORDEX snow water equivalent simulations at 0.11° (~12 km) show a much thicker average snowpack over the alpine ridge and shallower snowpack at low elevations with respect to the reference dataset. This behaviour, related to the RCM finer resolution, is sometimes smoothed out when snow water equivalent is spatially averaged over the Alpine domain (Figure 13). At regional scale, the annual cycle represented by ERA-Interim-driven RCMs results comparable to those found in the reference datasets and in GCMs. Important deviations from the reference datasets arise in GCM-driven RCM simulations (Figure 13). GCM-driven RCMs present stronger negative temperature bias and/or stronger positive precipitation biases, resulting in thicker snow water equivalent with respect to the ERA-Interim driven runs. Overall, GCM-driven RCM simulations tend to suffer the biases already present in the driver GCM and to reflect them in SNW fields.

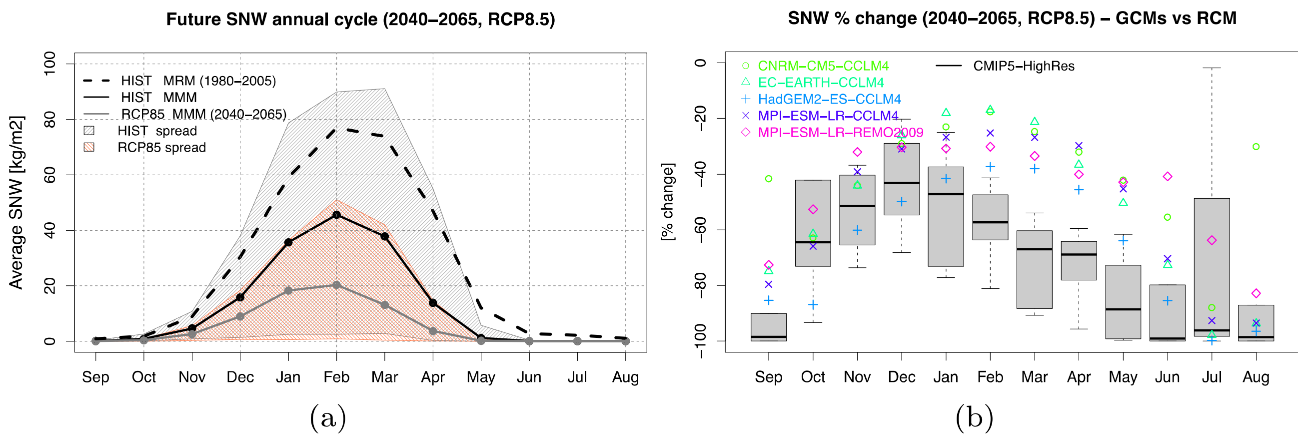

Figure 14. *(a) Annual cycle of snow water equivalent expected by the mid-21st century in the RCP8.5 scenario compared to the baseline 1980– 2005, as provided by the high-resolution CMIP5 models. (b) Percent change in snow water equivalent (2040–2065 average with respect to the baseline 1980–2005) as in the high-resolution CMIP5 GCMs (box plot) and RCM simulations.*

EURO-CORDEX RCMs future projections for mid 21st century in the RCP8.5 scenario show weaker snow reductions with respect to the coarser scale higher-resolution CMIP5 GCMs, especially in the spring season (Figure 14). While few regional models can have limited representativeness of the whole EURO-CORDEX ensemble and a larger set of simulations has to be considered as soon as they become available, this analysis highlights the large discrepancy among the considered datasets over the historical period and highlights the need of a reference observation-based product that could reliably represent the ground truth over the last decades.

Acknowledgements

The Arpa (Regional Agency for Environmental Protection) Piemonte and Aosta Valley are gratefully acknowledged for recovering and collecting meteorological data.

References

Acquaotta F., Fratianni S., Venema V., 2016. Assessment of parallel precipitation measurements networks in Piedmont, Italy. Int. J. Climatol., 36:3963–3974.

Acquaotta F, Fratianni S, Cassardo C, Cremonini R., 2009. On the continuity and climatic variability of the meteorological stations in Torino, Asti, Vercelli and Oropa. Meteorol. and Atmos. Phys., 103:279-287.

Aguilar E., Auer I., Brunet M., Peterson T. C., Wieringa, J., 2003. Guidance on metadata and homogenization. WMO-TD No. 1186.

Andreas E. L., Paulson C. A., Williams R. M., Lindsay R. W., Businger, J. A., 1979. The turbulent heat flux from Arctic leads. Bound. Layer Meteorol., 17, 57–91, doi:10.1007/BF00121937.

Arck M., Scherer D., 2002. Problems in the determination of sensible heat flux over snow. Geogr. Ann., 84A (3-4):157-169.

Aubinet M., Grelle A., Ibrom A., Rannik Ü., Moncrieff J., Foken T., Kowalski A. S., Martin P. H., Berbigier P., Bernhofer Ch., Clement R., Elbers J., Granier A., Grünwald T., Morgenstern K., Pilegaard K., Rebmann C., Snijders W., Valentini R., Vesala T., 2000. Estimates of the annual net carbon and water exchange of European forests: the EUROFLUX methodology. Adv. Ecol. Res., 30:114–175.

Balsamo G., Pappenberger F., Dutra E., Viterbo P., Van den Hurk B. J. J. M., 2011. A revised land hydrology in the ECMWF model: a step towards daily water flux prediction in a fully-closed water cycle, Hydrol. Proc., 25(7):1046-1054.

Baronetti A., Acquaotta F., Fratianni S., 2018. Rainfall variability from a dense rain gauges network in North-West of Italy. Climate Res., doi:10.3354/cr01517.

Bartelt P., Lehning M., 2002. A physical SNOWPACK model for the Swiss avalanche warning: Part I: numerical model. Cold Regions Sci. and Technol., 35(3):123-145.

Bavay M., Egger T., 2014. MeteoIO 2.4.2: a preprocessing library for meteorological data, Geoscientific Model Devel., 7(6), 3135-3151.

Beniston M., Farinotti D., Stoffel M., Andreassen L. M., Coppola E., Eckert N., Fantini A., Giacona F., Hauck, C., Huss, M., Huwald, H., Lehning M., López-Moreno, J. I., Magnusson J., Marty, C., Morán-Tejéda E., Morin S., Naaim M., Provenzale A., Rabatel A., Six D., Stötter J., Strasser U., Terzago S., Vincent C., 2018. The European mountain cryosphere: a review of its current state, trends, and future challenges, The Cryosphere, 12(2), 759.

Beniston M., 2012. Impacts of climatic change on water and associated economic activities in the Swiss Alps, J. Hydrol., 412:291-296.

Bertolotto P., Acquaotta F., Kermadi S., Fratianni S., 2018. Etude de la qualité des donnés neige en Italie: le cas de la Vallée d'Aoste. XXXIe colloque annuel de l'Association Internationale de Climatologie 4-7 Juillet 2018 – Nice, France.

Boni G., Castelli F., Gabellani S., Machiavello G., Rudari R., 2010. Assimilation of MODIS snow cover and real time snow depth point data in a snow dynamic model. Proc. IGARSS 2010, IEEE, 1788-1791.

Brauchli T., Trujillo E., Huwald H., Lehning, M., 2017. Influence of slope-scale snowmelt on catchment response simulated with the Alpine3D model. Water Resour. Res., 53, 10,723–10,739.

Brown R., Derksen C., Wang L., 2010. A multi-data set analysis of variability and change in Arctic spring snow cover extent, 1967–2008. Journal of Geophysical Research: Atmospheres, 115(D16).

Brown R. D., Mote P. W., 2009. The response of Northern Hemisphere snow cover to a changing climate, J. Climate, 22(8):2124-2145.

Campbell J. L., Mitchell M. J., Groffman P. M., Christenson L. M., Hardy J. P., 2005. Winter in northeastern North America: A critical period for ecological processes. Front. Ecol. Environ., 3:314-322.

Casella D., Panegrossi G., Sanò P., Marra A. C., Dietrich S., Johnson B. T., Kulie M. S., 2017. Evaluation of the GPM-DPR snowfall detection capability: Comparison with CloudSat-CPR, Atmos. Res., 197, 64-75, doi:10.1016/j.atmosres.2017.06.018.

Cassardo C., 2015. UTOPIA: The Manual of Version 2015, DOI:10.13140/RG.2.2.29664.38404 Available at https://www.researchgate.net/publication/323200198_UTOPIA_The_Manual_of_Version_2015.

Cassardo C., Park S. K., Galli M., Sungmin O., 2018. Climate change over the high-mountain versus plain areas: Effects on the land surface hydrologic budget in the Alpine area and northern Italy, Hydrol. Earth Syst. Sci., 22:3331-3350, https://doi.org/10.5194/hess-22-3331-2018.

Chen N. N., Guan D. X., Jin, C. J., Wang A., Wu J., Yuan F., 2011. Influences of snow event on energy balance over temperate meadow in dormant season based on eddy covariance measurements. J. Hydrol., 399:100–107.

Clarvis M. H., Fatichi S., Allan A., Fuhrer J., Stoffel M., Romerio F., Gaudard L., Burlando P., Beniston M., Xoplaki E., Toreti A., 2013. Governing and managing water resources under changing hydro-climatic contexts: The case of the upper Rhone basin, Environ. Sci. Policy, http://dx.doi.org/10.1016/j.envsci.2013.11.005.

Compo G. P., Whitaker J. S., Sardeshmukh P. D., Matsui N., Allan R. J., Yin, X., Gleason B. E., Vose R. S., Rutledge G., Bessemoulin P., Brönnimann S., Brunet M., Crouthamel R. I., Grant A. N., Groisman P. Y., Jones P. D., Kruk M. C., Kruger A. C., Marshall G. J, Maugeri M., Mok H. Y., Nordli Ø, Ross T. F., Trigo R. M., Wang X. L., Woodruff S. D., Worley S. J., 2011. The twentieth century reanalysis project. Quarterly Journal of the Royal Meteorological Society, 137(654):1-28.

Datt P., Srivastava P. K., Negi P. S., Satyawali P. K., 2008. Surface energy balance of seasonal snow cover for snow-melt estimation in N–W Himalaya. J. Earth Syst. Sci., 117 (5):567–573.

Dee D. P., Uppala S. M., Simmons A. J., Berrisford P., Poli P., Kobayashi S., Andrae U., Balmaseda M. A., Balsamo G., Bauer P., Bechtold P., Beljaars A.C.M., van de Berg L., Bidlot J., Bormann N., Delsol C., Dragani R., Fuentes M., Geer A. J., Haimberger L., Healy S. B., Hersbach H., Holm E. V., Isaksen L., K˚allberg P., K˙ohler M., Matricardi M., McNally A. P., Monge-Sanz B. M., Morcrette J. -J., Park B.-K., Peubey C., de Rosnay P., Tavolato C., Thèpaut J.-N. Vitart F. 2011. The ERA-Interim reanalysis: Configuration and performance of the data assimilation system, Quart. J. Roy. Meteor. Soc., 137(656):553-597.

Diffenbaugh N. S., Pal J. S., Trapp R. J., Giorgi F., 2005. Fine-scale processes regulate the response of extreme events to global climate change. Proc. Natl. Acad. Sci., 102(44):15774–15778.

Ebtehaj A. M., Kummerow C. D., 2017. Microwave retrievals of terrestrial precipitation over snow-covered surfaces: A lesson from the GPM satellite, Geophys. Res. Lett., 44, 6154-6162, doi:10.1002/2017GL073451.

Endrizzi S., Dall'Amico M., Gruber S., Rigon, R., 2014. GEOtop 2.0: simulating the combined energy and water balance at and below the land surface accounting for soil freezing, snow cover and terrain effects, Geoscientific Model Devel., 2014(7):2831-2857.

Essery R., Morin S., Lejeune Y., Ménard C. B., 2013. A comparison of 1701 snow models using observations from an alpine site, Adv. Water Resour., 55:131-148.

Fratianni S., Terzago S., Acquaotta F., Faletto M., Garzena D., Prola C., Barbero S., 2015. How snow and its physical properties change in a changing climate alpine context? in Engineering Geology for Society and Territory, Lollino G, Manconi A, Clague JW et al. (eds). Springer International Publishing, 57–60.

Frei C., Christensen J. H., Déqué M., Jacob D., Jones R. G., Vidale P. L., 2003. Daily precipitation statistics in regional climate models: Evaluation and intercomparison for the European Alps, J. Geophys. Res.: Atmospheres, 108(D3).

Galvagno M., Wohlfahrt G., Cremonese E., Rossini M., Colombo R., Filippa G., Julitta T., Manca G., Siniscalco C., Morra di Cella U., Migliavacca M., 2013. Phenology and carbon dioxide source/sink strength of a subalpine grassland in response to an exceptionally short snow season, Environ. Res. Lett., 8(2), 025008.

Hall D. K., Riggs G. A., 2007. Accuracy assessment of the MODIS snow products. Hydrological Processes: An International Journal, 21(12):1534-1547.

Hammerle A., Haslwanter A., Schmitt M., Bahn M., Tappeiner U., Cernusca A., Wohlfahrt G., 2007. Eddy covariance measurements of carbon dioxide, latent and sensible energy fluxes above a meadow on a mountain slope. Bound. Layer Meteorol., 122 (2):397–416.

Harmosnow. ESSEM COST Action ES1404 (2014-2018). A European network for a harmonised monitoring of snow for the benefit of climate change scenarios, hydrology and numerical weather prediction. http://www.harmosnow.eu.

Hayashi M., Van der Kamp G., Schmidt R., 2003. Focused infiltration of snowmelt water in partially frozen soil under small depressions. J. Hydrol., 270(3-4):214-229.

Haylock M., Hofstra N., Klein Tank A., Klok E., Jones P., New M., 2008. A European daily high-resolution gridded data set of surface temperature and precipitation for 1950–2006, J. Geophys. Res.-Atmos., 113, https://doi.org/doi:10.1029/2008JD010201 .

Helgason W. D., Pomeroy J. W., 2005. Uncertainties in estimating turbulent fluxes to melting snow in a mountain clearing. Proc. Eastern Snow Conf., 62:129-138.

Helgason W. D., Pomeroy J. W., 2012. Problems closing the energy balance over an homogeneous snow cover during midwinter. J. Hydrometeor., 13:557–572.

Hersbach H., Dee D., 2016. ERA5 reanalysis is in production. ECMWF Newsletter, 147, 7.

Hicks B. B., Martin H. C., 1972. Atmospheric turbulent fluxes over snow. Bound. Layer Meteorol., 2 (4):496-502.

Hiller R., Zeeman M., Eugster W., 2008. Eddy-covariance flux measurements in the complex terrain of an Alpine valley in Switzerland. Bound. Layer Meteorol., 127 (3):449–467.

IPCC, 2013: The physical science basis. Contribution of Working Group I to the Fifth Assessment Report of the Intergovernmental Panel on Climate Change. United Nations: Geneva.

Jepsen S. M., Molotch N. P., Williams M. W., Rittger K. E., Sickman J. O., 2012. Interannual variability of snowmelt in the Sierra Nevada and Rocky Mountains, USA: Examples from two alpine watersheds. Water Resour. Res., 48(2), W02529, doi:10.1029/2011WR011006.

Klein Tank A. M., Wijngaard J. B., Konnen G. P., Bohm R., Demaree G., Gocheva A., Mileta M., Pashiardis S., Hejkrlik L., Kern-Hansen C., Heino R., Bessemoulin P., Muller-Westermeier G., Tzanakou M., Szalai S., Palsdottir T., Fitzgerald D., Rubin S., Capaldo M., Maugeri M., Leitass A., Bukantis A., Aberfeld R., Van Engelen A. F. V., Forland E., Mietus M., Coelho F., Mares C., Razuvaev V., Nieplova E., Cegnar T., Lopez J. A., Dahlstrom B., Moberg A., Kirchhofer W., Ceylan A., Pachaliuk O., Alexander L. V., Petrovic P., 2002. Daily dataset of 20th-century surface air temperature and precipitation series for the European climate assessment. Int. J. Climatol. 22:1441–1453, doi:10.1002/joc.773.

Kulie M. S., Milani L., 2018. Seasonal variability of shallow cumuliform snowfall: A CloudSat perspective, Quart. J. Roy. Meteor. Soc., doi:10.1002/qj.3222.

Kulie M. S., Milani L., Wood N. B., Tushaus S. A., Bennartz R., L'Ecuyer T. S., 2016. A shallow cumuliform snowfall census using spaceborne radar, J. Hydrometeor., 17:1261-1279, doi:10.1175/JHM-D-15-0123.1.

Laviola S., Levizzani V., 2011. The 183-WSL fast rain rate retrieval algorithm. Part I: Retrieval design, Atmos. Res., 99:443-461, doi:10.1016/j.atmosres.2010.11.013.

Laviola S., Dong J., Kongoli C., Meng H., Ferraro R., Levizzani V., 2015. An intercomparison of two passive microwave algorithms for snowfall detection over Europe, IEEE Geosci. Remote Sensing Symp., 886-889, doi:10.1109/IGARSS.2015.7325907.

Lehning M., Bartelt P., Bethke S., 2004. Review of SNOWPACK and Alpine3D applications. In Snow Engineering, vol. V. (ed. Bartelt, P., E.E. Adams, M. Christen, R.L. Sack, and A. Sato). Leiden: Balkema Pubblishers, pp 299-307.

Leuning R., van Gorsel E., Massman W.J., Isaac, P. R., 2012. Reflections on the surface energy imbalance problem. Agr. Forest Meteorol. 156(0):65-74.

Levizzani V., Laviola S., Cattani E., 2011. Detection and measurement of snowfall from space, Remote Sens., 3(1):145-166, doi:10.3390/rs3010145.

Liu G., 2008. Deriving snow cloud characteristics from CloudSat observations, J. Geophys. Res., 113, D8, doi:10.1029/2007JD009766.

López-Moreno J. I., Fassnacht S. R., Beguería S., Latron, J. B. P., 2011. Variability of snow depth at the plot scale: implications for mean depth estimation and sampling strategies, The Cryosphere, 5:617-629, https://doi.org/10.5194/tc-5-617-2011.

López-Moreno J. I., Revuelto J., Gilaberte M., Morán-Tejeda E., Pons M., Jover E., Esteban P., García C., Pomeroy J. W., 2013. The effect of slope aspect on the response of snowpack to climate warming in the Pyrenees. Theor. Appl. Climatol. 117:207-219.

Marty C., Meister R., 2012. Long-term snow and weather observations at Weissfluhjoch and its relation to other high-altitude observatories in the Alps, Theor. Appl. Climatol., 110(4):573-583.

Meng H., Dong J., Ferraro R., Yan B. H., Zhao L. M., Kongoli C., Wang N.-Y., Zavodsky B., 2017. A 1DVAR-based snowfall rate retrieval algorithm for passive microwave radiometers, J. Geophys. Res., 122:6520-6540, doi:10.1002/2016JD026325.

Mignatti A., Casagrandi R., Provenzale A., von Hardenberg A., Gatto M., 2012. Sex-and age-structured models for Alpine ibex Capra ibex ibex population dynamics, Wildlife Biol., 18(3): 318-332.

Molotch N. P., Bales R. C., 2005. Scaling snow observations from the point to the grid element: Implications for observation network design, Water Resour. Res., 41, W11421, doi:10.1029/2005WR004229.

Mott R., Gromke C., Grünewald T., Lehning M., 2013. Relative importance of advective heat transport and boundary layer decoupling in the melt dynamics of a patchy snow cover. Adv. Water Resour., 55:88-97.

Mott R., Schlögl S., Dirks L., Lehning M., 2017. Impact of extreme land surface heterogeneity on micrometeorology over spring snow cover. J. Hydrometeor., 18 (10):2705-2722, doi:10.1175/JHM-D-17-0074.1.

Mudryk L. R., Derksen C., Kushner P. J., Brown, R., 2015. Characterization of Northern Hemisphere snow water equivalent datasets, 1981–2010. Journal of Climate, 28(20):8037-8051.

Nadeau D. F., Pardyjak E. R., Higgins C. W., Huwald H., Parlange M. B., 2013. Flow during the evening transition over steep alpine slopes. Quart. J. Roy. Meteor.. Soc., 139:607–624.

Nakai Y., Sakamoto T., Terajima T., Kitamura K., Shirai T., 1999. Energy balance above a boreal coniferous forest: a difference in turbulent fluxes between snow-covered and snow-free canopies. Hydrol. Process. 13:515–529.

Nilsson C., Malm Renöfält B., 2008. Linking flow regime and water quality in rivers: a challenge to adaptive catchment management. Ecology and Society 13(2): 18. [online] URL: http://www.ecologyandsociety.org/vol13/iss2/art18/].

Oldroyd H.L., Pardyjak E. R., Huwald H., Parlange Marc B., 2016. Adapting tilt corrections and the governing flow equations for steep, fully three-dimensional, mountainous terrain Boundary-Layer Meteorol., 159:539–565.

Panegrossi G., Rysman J.-F., Casella D., Marra A. C., Sanò P., Kulie M. S., 2017. CloudSat-based assessment of GPM Microwave Imager snowfall observation capabilities, Remote Sens., 12, 1263, doi:10.3390/rs9121263.

Peterson T. C., Easterling D., Karl T., Groisman P., Nicholls N., Plummer N., Torok S., Auer I., Boehm R., Gullet D., Vincent L., Heino R., Tuomenvirta H., Mestre O., Szentimrey T., Salinger J., Førland E. J., Hanssen-Bauer I., Alexandersson H., Jones P., Parker D., 1998: Homogeneity adjustment of in situ atmospheric climate data: a review. Int. J. Climatol., 18:1493–1517.

Pettorelli N., Pelletier F., Hardenberg A. V., Festa-Bianchet M., Côté S. D., 2007. Early onset of vegetation growth vs. rapid green-up: Impacts on juvenile mountain ungulates, Ecology, 88(2):381-390.

Piazzi G., Thirel G., Campo L., Gabellani S., 2018. A particle filter scheme for multivariate data assimilation into a point-scale snowpack model in an Alpine environment, The Cryosphere, 12:2287-2306, doi:10.5194/tc-12-2287-2018.

Reba M. L., Link T. E., Marks D., Pomeroy J., 2009. An assessment of corrections for eddy covariance measured turbulent fluxes over snow in mountain environments. Water Resour. Res., 45, W00D38, doi:10.1029/2008WR007045.

Reba M.L., Marks D., Seyfried M., Winstral A., Kumar M., Flerchinger G., 2011. A long-term data set for hydrologic modeling in a snow-dominated mountain catchment. Water Resour. Res., 47, W07702. doi:10.1029/2010WR010030.

Rienecker M. M., Suarez M. J., Gelaro R., Todling R., Bacmeister J., Liu, E., Bosilovich M. G., Schubert S. D., Takacs L., Gi-Kong Kim, Bloom S., Chen J., Collins D., Conaty A., da Silva A., Gu W., Joiner J., Koster R. D., Lucchesi R., Molod A., Owens T., Pawson S., Pegion P., Redder C. R., Reichle R., Robertson F. R., Ruddick A. G., Sienkiewicz M., Woollen J., 2011. MERRA: NASA's modern-era retrospective analysis for research and applications. Journal of climate, 24(14):3624-3648.

Rodell M., Houser P. R., Jambor U., Gottschalck J., Mitchell K., Meng C.-J., Arsenault K., Cosgrove B., Radakovich J., Bosilovich M., Entin J. K., Walker J. P., Lohmann D., Toll D., 2004. The Global Land Data Assimilation System, Bull. Amer. Meteor. Soc., 85(3):381-394.

Rui H., Beaudoing, H., 2018. README Document for NASA GLDAS Version 2 Data Products, Goddart Earth Sciences Data and Information Services Center (GES DISC).

Saitoh T. M., Tamagawa I., Muraoka H., Koizumi H., 2011. Energy balance closure over a cool temperate forest in steeply sloping topography during snowfall and snow-free periods. J.Agr. Meteor., 67(3):107-116.

Saha, S., Moorthi, S., Pan, H. L., Wu, X., Wang, J., Nadiga, S., Tripp P., Kistler R., Woollen J., Behringer D., Liu H., Stokes D., Grumbine R., Gayno G., Wang J., Hou Y. –T., Chuang H., Juang H. –M. H., Sela J., Iredell M., Treadon R., Kleist D., Van Delst P., Keyser D., Derber J., Ek M., Meng J., Wei H., Yang R., Lord S., van den Dool H., Kumar A., Wang W., Long C., Chelliah M., Xue Y., Huang B., Schemm J. –K., Ebisuzaki W., Lin R., Xie P., Chen M., Zhou S., Higgins W., Zou c. –Z., Liu Q., Chen Y., Han Y., Cucurull L., Reynolds R. W., Rutledge G., Goldberg M., 2010. The NCEP climate forecast system reanalysis. Bulletin of the American Meteorological Society, 91(8):1015-1058.

Salzmann N., Huggel C., Rohrer M., Stoffel M., 2014. Data and knowledge gaps in glacier, snow and related runoff research–A climate change adaptation perspective. Journal of Hydrology, 518:225-234.

Schaefli B., Hingray B., Musy A., 2007. Climate change and hydropower production in the Swiss Alps: quantification of potential impacts and related modeling uncertainties. Hydrol. Earth Syst. Sci., 11:1191–1205.

Schaefli B., Manso P.; Fischer M., Huss M., Farinotti D., 2019. The role of glacier retreat for Swiss hydropower production. Renew. Energy, 132:615-627. doi: 10.1016/j.renene.2018.07.104

Skofronick-Jackson G., Johnson B. T., Munchak S. J., 2013. Detection thresholds of falling snow from satellite-borne active and passive sensors, IEEE Trans. Geosci. Remote Sens., 15:4177 – 4189, doi:10.1109/TGRS.2012.2227763.

Skofronick-Jackson G., Kim M.-J., Weinman J. A., Chang D.-E., 2004. A physical model to determine snowfall over land by microwave radiometry, IEEE Trans. Geosci. Remote Sens., 42:1047-1058, doi:10.1109/TGRS.2004.825585.

Smith C. D., Kontu A., Laffin R., Pomeroy J. W., 2017. An assessment of two automated snow water equivalent instruments during the WMO Solid Precipitation Intercomparison Experiment, The Cryosphere, 11:101-116, doi:10.5194/tc-11-101-2017.

Sneyers, 1990. On the statistical analysis of series of observations. Geneva, WMO N 143, p 192.

SPICE. WMO Solid Precipitation InterComparison Experiment (2012-2015). http://www.wmo.int/pages/prog/www/IMOP/intercomparisons/SPICE/SPICE.html.

Stössel F., Guala M., Fierz C., Manes C., Lehning, M., 2010. Micrometeorological and morphological observations of surface hoar dynamics on a mountain snow cover. Water Resour. Res., 46, W04511, doi:10.1029/2009WR008198.

Terzago S., Cremonini R., Cassardo C., Fratianni S., 2012. Analysis of snow precipitation during the period 2000–2009 and evaluation of a snow cover algorithm in the South Western Italian Alps. Geografia Fisica e Dinamica Quaternaria, 35:91-99.

Terzago S., Fratianni S., Cremonini R. 2013. Winter precipitation in Western Italian Alps (1926-2010): trends and connections with the North Atlantic/Arctic Oscillation. Meteorol. Atmos. Phys., 119:125-136.

Terzago S., von Hardenberg J., Palazzi E., Provenzale, A., 2017. Snow water equivalent in the Alps as seen by gridded data sets, CMIP5 and CORDEX climate models, The Cryosphere, 11:1625-1645, https://doi.org/10.5194/tc-11-1625-2017 .

Turnipseed A. A., Anderson D. E., Blanken P. D., Baugh W., Monson R. K., 2003. Airflows and turbulent flux measurements in mountainous terrain. Part 1: canopy and local effects. Agr. Forest Meteor., 119:1–21.

Twine T. E., Kustas W. P., Norman J. M., Cook D. R., Houser P. R., Meyers T. P., Prueger J. H., Starks P. J., Wesely M. L., 2000. Correcting eddy-covariance flux underestimates over a grassland. Agr. Forest Meteor., 103(3):279-300.

Wilson K. B., Goldstein A., Falge E., Aubinet M., Baldocchi D., Berbigier P., Bernhofer C., Ceulemans R., Dolman H., Field C., Grelle A., Ibrom A., Law B. E., Kowalski A., Meyers T., Moncrieff J., Monson R., Oechel W., Tenhunen J., Valentini R., Verma S., 2002. Energy balance closure at FLUXNET sites. Agr. Forest. Meteor., 113:223–243.

Wilson K. B., Baldocchi D.D., 2000. Seasonal and interannual variability of energy fluxes over a broadleaved temperate deciduous forest in North America. Agric. For. Meteor., 100:1–18.

You Y., Wang N.-Y., Ferraro R., Rudlosky S., 2017. Quantifying the snowfall detection performance of the GPM Microwave Imager channels over land, J. Hydrometeor., 18:729-751, doi:10.1175/JHM-D-16-0190.1.

Yue S., Wang C., 2004. The Mann-Kendall Test Modified by Effective Sample Size to Detect Trend in Serially Correlated Hydrological Series. Water Resour. Manag., 18:201–218.

Zhang X., Vincent L. A., Hogg W. D., Niitsoo A., 2000. Temperature and precipitation trends in Canada during the 20th century. Atmosphere-Ocean, 38:395–429.